The Astrophysical Journal, 737:96 (17pp), 2011 August 20 doi:10.1088/0004-637X/737/2/96

*HERSCHEL** MEASUREMENTS OF MOLECULAR OXYGEN IN ORION

Paul F. Goldsmith[1], René Liseau[2], Tom A. Bell[3], John H. Black[2], Jo-Hsin Chen[1], David Hollenbach[4], Michael J. Kaufman[5], Di Li[1], Dariusz C. Lis[6], Gary Melnick[7], David Neufeld[8], Laurent Pagani[9], Ronald Snell[10], Arnold O. Benz[11], Edwin Bergin[12], Simon Bruderer[11], Paola Caselli[13], Emmanuel Caux[14,15], Pierre Encrenaz[9], Edith Falgarone[16], Maryvonne Gerin[16], Javier R. Goicoechea[3], Åke Hjalmarson[2], Bengt Larsson[17], Jacques Le Bourlot[18], Franck Le Petit[18], Massimo De Luca[18], Zsofia Nagy[19], Evelyne Roueff[18], Aage Sandqvist[17], Floris van der Tak[19], Ewine F. van Dishoeck[20,21], Charlotte Vastel[14,15], Serena Viti[22], and Umut Yıldız[20]
[1] Jet Propulsion Laboratory, California Institute of Technology, 4800 Oak Grove Drive, Pasadena, CA 91109, USA; Paul.F.Goldsmith@jpl.nasa.gov
[2] Department of Earth & Space Sciences, Chalmers University of Technology, Onsala Space Observatory, SE-439 92 Onsala, Sweden
[3] Centro de Astrobiología, CSIC–INTA, 28850 Madrid, Spain
[4] SETI Institute, Mountain View, CA 94043, USA
[5] Department of Physics and Astronomy, San José State University, San Jose, CA 95192, USA
[6] California Institute of Technology, Cahill Center for Astronomy and Astrophysics 301-17, Pasadena, CA 91125, USA
[7] Harvard-Smithsonian Center for Astrophysics, 60 Garden Street, MS 66, Cambridge, MA 02138, USA
[8] Department of Physics and Astronomy, Johns Hopkins University, 3400 North Charles Street, Baltimore, MD 21218, USA
[9] LERMA & UMR8112 du CNRS, Observatoire de Paris, 61 Av. de l'Observatoire, 75014 Paris, France
[10] Department of Astronomy, University of Massachusetts, Amherst, MA 01003, USA
[11] Institute of Astronomy, ETH Zurich, Zurich, Switzerland
[12] Department of Astronomy, University of Michigan, 500 Church Street, Ann Arbor, MI 48109, USA
[13] School of Physics and Astronomy, University of Leeds, Leeds, UK
[14] Université de Toulouse; UPS-OMP; IRAP; Toulouse, France
[15] CNRS; IRAP; 9 Av. Colonel Roche, BP 44346, F-31028 Toulouse Cedex 4, France
[16] LRA/LERMA, CNRS, UMR8112, Observatoire de Paris & École Normale Supérieure, 24 rue Lhomond, 75231 Paris Cedex 05, France
[17] Stockholm Observatory, Stockholm University, AlbaNova University Center, SE-106 91 Stockholm, Sweden
[18] Observatoire de Paris, LUTH, Paris, France
[19] SRON Netherlands Institute for Space Research, P.O. Box 800, 9700 AV, and Kapteyn Astronomical Institute, University of Groningen, Groningen, The Netherlands
[20] Leiden Observatory, Leiden University, P.O. Box 9513, 2300 RA, Leiden, The Netherlands
[21] Max-Planck-Institut für Extraterrestrische Physik, Giessenbachstrasse 1, 85748, Garching, Germany
[22] Department of Physics and Astronomy, University College London, London, UK
Received 2011 May 8; accepted 2011 June 10; published 2011 August 8

ABSTRACT

We report observations of three rotational transitions of molecular oxygen (O_2) in emission from the H_2 Peak 1 position of vibrationally excited molecular hydrogen in Orion. We observed the 487 GHz, 774 GHz, and 1121 GHz lines using the Heterodyne Instrument for the Far Infrared on the *Herschel Space Observatory*, having velocities of 11 km s^{-1} to 12 km s^{-1} and widths of 3 km s^{-1}. The beam-averaged column density is $N(O_2) = 6.5 \times 10^{16}$ cm^{-2}, and assuming that the source has an equal beam-filling factor for all transitions (beam widths 44, 28, and 19″), the relative line intensities imply a kinetic temperature between 65 K and 120 K. The fractional abundance of O_2 relative to H_2 is (0.3–7.3) $\times 10^{-6}$. The unusual velocity suggests an association with a ∼5″ diameter source, denoted Peak A, the Western Clump, or MF4. The mass of this source is $\sim 10\,M_\odot$ and the dust temperature is $\geqslant$150 K. Our preferred explanation of the enhanced O_2 abundance is that dust grains in this region are sufficiently warm ($T \geqslant 100$ K) to desorb water ice and thus keep a significant fraction of elemental oxygen in the gas phase, with a significant fraction as O_2. For this small source, the line ratios require a temperature $\geqslant$180 K. The inferred O_2 column density $\simeq 5 \times 10^{18}$ cm^{-2} can be produced in Peak A, having $N(H_2) \simeq 4 \times 10^{24}$ cm^{-2}. An alternative mechanism is a low-velocity (10–15 km s^{-1}) C-shock, which can produce $N(O_2)$ up to 10^{17} cm^{-2}.

Key words: astrochemistry – ISM: abundances – ISM: individual objects (Orion) – ISM: molecules – submillimeter: ISM

Online-only material: color figures

1. INTRODUCTION

1.1. Chemistry of Oxygen in Dense Interstellar Clouds

Oxygen is the third most abundant element in the universe, and its form in different regions is thus of considerable astronomical importance. Whittet (2010) has recently reexamined the question of oxygen abundance as a function of density in the interstellar medium (ISM) and finds that a large fraction of oxygen is unaccounted for at the higher densities which generally correspond to the molecular ISM. Models of gas-phase chemistry that do not treat the condensation of species as icy mantles on grains have predicted molecular oxygen (O_2) to be abundant in well-shielded regions, with $X(O_2) = N(O_2)/N(H_2)$ greater than 10^{-5}, and thus the most abundant molecular species after H_2 and CO, with predicted abundance exceeding that for water (Herbst & Klemperer 1973; Prasad & Huntress 1980; Graedel et al. 1982; Leung et al. 1984; Langer & Graedel 1989; Bergin et al. 1995; Maréchal et al. 1997b). The conditions that generally (but not in every model) maximize the abundance of O_2 are low metal abundance (consistent with depletion on grains), high

* *Herschel* is an ESA space observatory with science instruments provided by European-led Principal Investigator consortia and with important participation from NASA.

densities, and sufficient time for oxygen chemistry to come into steady state.

The gas-phase chemistry of O_2 in dense clouds is relatively simple. Formation of O_2 is initiated by the reaction of atomic oxygen with H_3^+ to form OH^+. H_3^+ is produced by cosmic ray ionization of H_2 and subsequent reaction of the resulting H_2^+ with H_2. The OH^+ reacts with H_2 to produce H_2O^+, and by a second reaction, H_3O^+. This ion dissociatively recombines with an electron, and the two channels of interest result in H_2O and OH. The latter species can react with an oxygen atom to form O_2.

Uncertainties in several of the key reaction rates have been reduced by laboratory measurements. The dissociative recombination of H_3O^+ has been measured using heavy-ion storage rings by Vejby-Christensen et al. (1997), Jensen et al. (2000), and Neau et al. (2000). The reaction rate for all three of these measurements is in reasonable agreement in magnitude and temperature dependence, with a large thermal rate coefficient $\alpha \simeq 3 \times 10^{-6}$ cm^3 s^{-1} at 50 K, and a temperature dependence $\propto T^{-0.8}$. These results are consistent with the earlier results by Mul et al. (1983) obtained using a different technique. The branching ratio has been a subject of some uncertainty, the papers cited above all put the fraction of the recombinations that result in production of OH in the range $0.5 \leqslant f(\mathrm{OH}) \leqslant 0.7$. Thus, the effective rate coefficient for the formation of OH by dissociative recombination of H_3O^+ at the temperature of dense molecular clouds is about 2×10^{-6} cm^3 s^{-1}.

The rate at low temperatures of the reaction OH + O $\rightarrow$ O_2, the final step in the production of molecular oxygen, has been the subject of some controversy. Theoretical calculations by Harding et al. (2000) were in moderately good agreement with the measurements for temperatures between 150 K and 500 K (Howard & Smith 1981; Smith & Stewart 1994), and indicated the peak value of the rate coefficient to be $k = 5.5 \times 10^{-11}$ cm^3 s^{-1} at $\simeq$80 K, with a factor $\simeq$2 reduction at 10 K and 1000 K. Measurements by Carty et al. (2006) sampled a range of temperatures, but these authors recommended the use of a single value, $k = 3.5 \pm 1.0 \times 10^{-11}$ cm^3 s^{-1} over the temperature range 39 K $\leqslant T \leqslant$ 142 K.

The calculations by Xu et al. (2007) suggested a rate that, while only somewhat lower than that of Carty et al. (2006) at temperatures above 80 K, fell dramatically at lower temperatures. This opened the possibility that the O_2 abundance in cooler clouds would be much lower than predicted by the above astrochemical models. However, more elaborate quantum mechanical calculations by Quémener et al. (2008) showed a relatively weak temperature dependence, and a rate coefficient at 10 K that is 70 times larger than predicted by Xu et al. (2007).

Recent quantum calculations by Lique et al. (2009a) give rate coefficients that are a factor $\simeq$2 greater than the measurements of Carty et al. (2006) over their temperature range. The rate coefficients from these latest theoretical calculations do fall at temperatures below 30 K, but even at 10 K are $\geqslant 3 \times 10^{-11}$ cm^3 s^{-1}, thus guaranteeing that the OH + O $\rightarrow$ O_2 + H reaction will not be a low-temperature bottleneck for O_2 production. The agreement between measured and theoretical calculations of the reaction rates suggests that the O_2 production rate is reasonably well understood and confirms the purely gas-phase chemistry prediction of large $X(O_2)$ in all but possibly the coldest clouds.

The expectation of a high abundance of O_2 had previously been an impetus to include this species in calculations of gas-phase cooling (Goldsmith & Langer 1978), and it was found to be moderately important at intermediate densities, despite its weak magnetic dipole transitions. The major obstacle to studies of astronomical O_2 is the strong absorption by this same species in Earth's atmosphere. The large-scale height of O_2 compared to that of H_2O means that even going to high altitude sites does not allow for observations of Galactic O_2 in the ISM, where only the energy levels producing millimeter and submillimeter rotational transitions will likely be populated. Although absorption observations of UV transitions are possible from space (Smith et al. 1984), clouds with sufficient column density to have detectable transitions of O_2 are likely to have sufficiently large dust opacities that such observations will prove difficult.

1.2. Grain Surface Oxygen

A possibility that must be considered is that O_2 is resident on dust grain surfaces. Solid O_2 has been searched for in interstellar clouds through its weak feature at 6.45 μm, with negative results (Vandenbussche et al. 1999). The most stringent abundance limits come from analysis of the solid ^{13}CO line profiles in low- and high-mass star-forming regions, which indicate solid O_2 concentrations of less than 10% with respect to water ice (Boogert et al. 2002; Pontoppidan et al. 2003). Taking a typical water ice abundance of 10^{-4} relative to H_2, this indicates solid O_2/gas-phase H_2 abundance ratios $\leqslant 10^{-5}$ within a factor of two. Thus, at most 10% of elemental oxygen is locked up in O_2 on grain surfaces.

Laboratory measurements show that solid O_2 ice is only slightly less volatile than CO ice with a binding energy of $\sim$900 K and thermally evaporates at 16–18 K under typical interstellar conditions (Acharyya et al. 2007). If trapped in water ice, a small fraction of O_2 can desorb at higher temperatures together with H_2 (Collings et al. 2004). Once on the grains, solid O_2 is chemically active. A number of recent laboratory experiments have demonstrated that O_2 is rapidly hydrogenated by atomic H to form OH, H_2O_2, and H_2O in ices, even at temperatures as low as 12 K (Miyauchi et al. 2008; Ioppolo et al. 2008, 2010). Some gas-phase O_2 can also be produced by photodesorption of H_2O ice at high temperatures (Öberg et al. 2009a). The nondetection of solid O_2 on grain surfaces is thus reasonable, and the amount of molecular oxygen on dust grains is not a major contributor to the overall oxygen budget in dense interstellar clouds.

1.3. Searches for Molecular Oxygen

Several different techniques have been utilized in the search for interstellar O_2. In general, these normalize the derived column density (or upper limit thereto) to that of standard tracer, generally an isotopologue of carbon monoxide, from which the molecular hydrogen column density can be derived. The resultant fractional abundance of or upper limit to the fractional abundance of O_2 is obtained assuming that the distributions of the species are the same. The isotopologue $^{16}O^{18}O$ has levels and transitions that are not allowed for the homonuclear common isotopologue, and some of these are at frequencies at which the atmosphere is reasonably transparent, notably the $(N, J) = (2,1) \rightarrow (0,1)$ transition at 233.95 GHz (Black & Smith 1984; Maréchal et al. 1997c). Ground-based observational searches for $^{16}O^{18}O$ have been carried out with nondetections giving upper limits $X(O_2)$ somewhat lower than those for CO (Goldsmith et al. 1985; Liszt & Vanden Bout 1985; Liseau et al. 2010). A ground-based search (Pagani et al. 1993) yielded a tentative detection in one source that was not confirmed by further observations (Maréchal et al. 1997a) with significantly improved

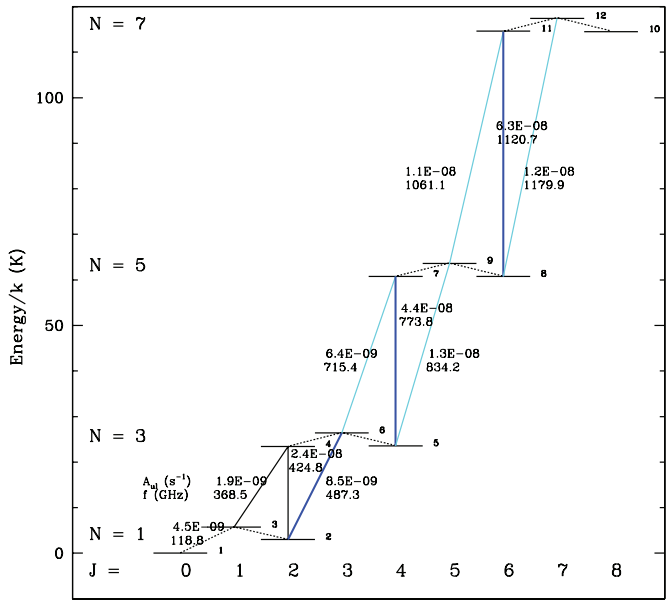

Figure 1. Lower rotational energy levels and transitions of O_2. Each level is described by its rotational quantum number N and total angular momentum quantum number J, with $J = N-1, N, N+1$. This designation applies rigorously only to Hund's case (b), as described by Lique (2010), but is generally used to designate O_2 levels. The frequencies of the allowed transitions are given in GHz, together with the spontaneous decay coefficients in s^{-1}. Transitions with $\Delta N = 0$ are indicated by dotted lines; these have frequencies in the vicinity of 60 GHz with the exception of the $(N, J) = (1, 1) \rightarrow (1, 0)$ transition at a frequency of 118.8 GHz. The seven transitions that fall in the frequency range covered by *Herschel* HIFI are shown in color, with the three relatively strong transitions discussed here (487, 774, and 1121 GHz) shown in heavy dark blue. See Maréchal et al. (1997a) for additional details.

limits. Fuente et al. (1993) searched for the 234 GHz transition of $^{16}O^{18}O$ in three dark clouds and measured 1σ upper limits $N(O_2)/N(CO) \leqslant 0.15$, 0.19, and 0.29 for in TMC2, L134N, and B335, respectively.

The common isotopologue of molecular oxygen can be observed using ground-based telescopes from sources having velocities sufficient to Doppler-shift the observed frequency "out from under" the pressure-broadened terrestrial O_2 absorption. The lower rotational transitions of O_2 referred to here are shown in Figure 1. This technique has been used to search for O_2 in the galaxy NGC 7674 by Liszt (1985), using the redshifted 119 GHz line, who found $X(O_2) \leqslant 1.4 \times 10^{-5}$ (1σ). Goldsmith & Young (1989) searched for the 119 GHz O_2 transition in the galaxy VII Zw 31, determining a 1σ upper limit $X(O_2) \leqslant 4 \times 10^{-6}$. Combes et al. (1991) searched for O_2 in NGC 6240 as well as $^{16}O^{18}O$ in two Galactic sources, obtaining upper limits $X(O_2) \leqslant 1 \times 10^{-6}$. Liszt (1992) added three galaxies having recession velocities between 8800 and 12,000 km s^{-1} and carried out additional observations of NGC 7674, finding $N(O_2)/N(CO) \leqslant 0.05$ at the 1σ level. Combes & Wiklind (1995) searched for redshifted 368 GHz and 424 GHz O_2 lines in the BL Lac object B0218+357 having $z = 0.685$, determining $N(O_2)/N(CO) \leqslant 0.014$. Combes et al. (1997) observed this same source, but in the 56.3 and 119 GHz O_2 transitions, and obtained an improved upper limit $N(O_2)/N(CO) \leqslant 2 \times 10^{-3}$. Frayer et al. (1998) searched for O_2 in Markarian 109, obtaining an upper limit $N(O_2)/N(CO) \leqslant 0.31$ in this low-metallicity galaxy. All of the above ground-based observations had angular resolutions $\leqslant 1'$.

Observations of O_2 are possible from balloon altitude for sources within the Milky Way with sufficiently large velocities. Olofsson et al. (1998) searched for the 424 GHz transition of O_2 from an altitude of 39.5 km with a 60 cm telescope giving a beam width $\simeq 5'$. They did not detect O_2, but were able to determine upper limits in two sources, NGC7538 and W51, with $N(O_2)/N(CO) \leqslant 0.1$. Since $X(CO)$ is expected to be $\simeq 10^{-4}$ in warm regions, these limits correspond to $X(O_2) \leqslant 10^{-5}$.

The best environment for searching for molecular oxygen in the Milky Way as well as other galaxies is clearly above Earth's atmosphere, from a spacecraft. Out of a number of proposals, two modest-sized space missions dedicated to submillimeter-wavelength spectroscopy have been successfully developed and operated. The first of these was NASA's *Submillimeter Wave Astronomy Satellite* (*SWAS*) launched in 1998, which observed the 487 GHz O_2 line (Melnick et al. 2000) with a beam width $3'.5 \times 5'$. Numerous clouds in the Milky Way were observed, but there were no definitive detections of O_2. Upper limits reported by Goldsmith et al. (2000) were as low as $X(O_2) \leqslant 2.6 \times 10^{-7}$, and a combination of data from nine sources yielded $\langle X(O_2) \rangle = [0.33 \pm 1.6(3\sigma)] \times 10^{-7}$.

The *Odin* satellite (Nordh et al. 2003) was launched in 2001. It was equipped with a larger antenna and more flexible receiver system than those of *SWAS*. Observations of O_2 were primarily of the 119 GHz transition with a beam width of $9'$ (Pagani et al. 2003), giving upper limits to $X(O_2)$ in half of the sources being as low as 10^{-7}. This survey included relatively warm giant molecular clouds (GMCs), but due to the low energy of the upper level of this transition, the upper limits for O_2 in dark clouds were significantly lower than those obtained with *SWAS*. A study of the Sgr A cloud in the Galactic center yielded a 3σ upper limit $X(O_2) \leqslant 1.2 \times 10^{-7}$ (Sandqvist et al. 2008). Wilson et al. (2005) used *Odin* to search for O_2 in the Small Magellanic Cloud galaxy, and after 39 hr of integration obtained a 3σ upper limit $X(O_2) \leqslant 1.3 \times 10^{-6}$ in this source that has a (total) oxygen abundance less than 0.2 of that in the Orion Nebula in the Milky Way.

A very deep *SWAS* integration on a mosaic of positions in the ρ Ophiuchi cloud yielded a detection of the 487 GHz line at modest statistical significance (Goldsmith et al. 2002). The 5.5 km s^{-1} velocity of the observed emission line fell within the redshifted wing of a low-velocity molecular outflow. Since the column density of the outflowing gas is modest, the fractional abundance of O_2 derived was quite large, $X(O_2) = 1 \times 10^{-5}$. This result was not confirmed by subsequent *Odin* observations of the 119 GHz line, which did detect an emission feature, but at a velocity of 3.5 km s^{-1}, and line width of 1.5 km s^{-1}, corresponding to the characteristics of the quiescent cloud rather than the outflow. The line is quite weak and due to the large column density of the bulk of the source, the derived fractional abundance of O_2, $X(O_2) = 5 \times 10^{-8}$ (Larsson et al. 2007), is relatively low. The consensus emerging from these observations of O_2 is that the abundance of this species in a variety of different types of molecular clouds is dramatically lower than predictions of standard gas-phase chemistry. Instead of an abundance $X(O_2) \simeq 10^{-5}$, the upper limits are as low as 10^{-7}, only slightly above the level of the *Odin* ρ Ophiuchi detection.

However, even preceding the arrival of data from space missions, there had been theoretical models of the ISM that predicted lower O_2 abundances. Xie et al. (1995) investigated turbulent diffusion, which in principle could accelerate mixing of material from UV-irradiated cloud edges with the material deeper inside. The result is a reduction in the abundances of certain molecules including O_2. A model employing circulation has been developed by Chièze & Pineau des Forêts (1989),

which can result in a significant reduction in the abundance of O_2 if the characteristic circulation time is as short as 10^6 yr. Le Bourlot et al. (1995) studied a bistability in interstellar chemistry that under certain conditions can result in a high ionization phase in which the abundance of O_2 is reduced by a factor $\simeq$100 relative to standard gas-phase chemistry. This is largely restricted to regions of low-to-moderate density, but can be favored by high cosmic ray fluxes.

Results from *SWAS* and *Odin* indicated that the low abundance of O_2 is widespread, and included very well shielded regions of high density with $n(H_2) \geqslant 10^4$ cm^{-3}. Additionally, the abundance of H_2O was found to be substantially below that expected from gas-phase chemistry models. To address this, Bergin et al. (2000) developed a model invoking depletion of atomic oxygen onto dust grains, and conversion to water ice remaining on the grain surface. This model results in an increase of the gas-phase C/O ratio, which has the effect of dramatically reducing the fractional abundance of O_2 deep inside clouds. Hollenbach et al. (2009) later showed that at intermediate depths ($A_V \sim$ 2–8), photodesorption of water ice from grains maintained a sufficiently high gas-phase abundance of elemental oxygen that abundances $X(O_2) \sim 3 \times 10^{-7}$ were achieved in these regions, independent of the gas density or incident ultraviolet flux.

The situation regarding O_2 has remained sufficiently puzzling that an Open Time Key Program (Herschel Oxygen Project) was proposed and selected to carry out a survey of warm molecular clouds in three rotational transitions of this elusive species. This paper presents the results for some of the observations in Orion, which we give in Section 2. In Section 3, we discuss the identification as O_2. In Section 4, we discuss collisional excitation of O_2, the source temperature, and O_2 column density derived assuming the source fills all the Heterodyne Instrument for the Far Infrared (HIFI) beams. In Section 5, we analyze the effects of beam filling and source offset, and discuss the column density and fractional abundance of O_2 that apply to different possible source geometries. We discuss shocks and warmed grains as sources of the observed O_2 in Section 6. In Section 7, we present a summary of our results and conclusions.

2. HIFI OBSERVATIONS

2.1. Data Taking

These data were taken with the HIFI (de Graauw et al. 2010) on the *Herschel Space Observatory* (Pilbratt et al. 2010). The observations were carried out on operational days 291, 297, 474, 504, and 505 in 2010 March, August, September, and October. The position observed is the direction of the north west maximum of H_2 rovibrational emission (Beckwith et al. 1978). The coordinates are $\alpha_{J2000} = 5^h35^m13\overset{s}{.}7$, $\delta_{J2000} = -05°22'09''$. Double beam switching was employed. For observations of Orion the spacecraft pointing constraints meant that the reference positions were located within 10° of an east–west line, with one position being 3′ east of the source position and the other being symmetrically located to the west. Eight settings of the local oscillator were used to enable sideband deconvolution. HIFI band 1a was used for the 487 GHz observations, band 2b for the 774 GHz observations, and band 5a for the 1121 GHz observations. Observations of the $J = 7$–6 C^{17}O transition were obtained simultaneously with the 774 GHz O_2 data, and the results are discussed in Section 3.2.

The total (on-source + off-source) integration time for the 487 GHz observations was 440 minutes for H polarization and 398 minutes for the V polarization, due to the failure of one segment of the observations for the latter. The integration times were 430 and 409 minutes for the 774 GHz and 1121 GHz observations, respectively. The full width at half maximum (FWHM) beam width is 44″ at 487 GHz, 28″ at 774 GHz, and 19″ at 1121 GHz, while the main beam efficiency, ϵ_{MB}, is equal to 0.76, 0.75, and 0.64 at the three frequencies, respectively (Olberg 2010). These long integrations provided a test of the performance of the HIFI radiometers. As discussed in Appendix A, the noise in the final spectra is a factor ∼1.6 greater than expected theoretically. Figure 2 shows the HIFI beams on an image of the H_2 emission in Orion and indicates some of the compact sources in the vicinity.

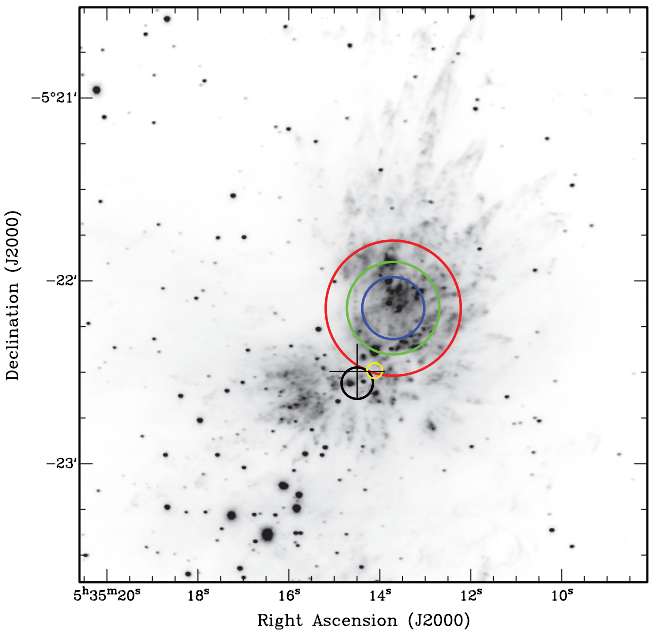

Figure 2. Image of vibrationally excited 2 μm H_2 emission in Orion (from Bally et al. 2011). The coordinates of H_2 Peak 1 toward which *Herschel* was pointed for these observations are $\alpha_{J2000} = 5^h35^m13\overset{s}{.}7$, $\delta_{J2000} = -5°22'09''$. The three circles indicate the FWHM beam sizes at the three observed frequencies: 44″ at 497 GHz, 28″ at 774 GHz, and 19″ at 1121 GHz. The position of the Hot Core ($\alpha_{J2000} = 5^h35^m14\overset{s}{.}5$, $\delta_{J2000} = -5°22'33\overset{''}{.}6$) is indicated by the black circle 10″ in diameter, approximately the size of this region (Wilson et al. 2000). The Peak A–Western Clump–MF4–Cnt D source (see references in the text) is indicated by the yellow circle, 5″ in diameter. The infrared source IRc2 (Downes et al. 1981) is indicated by the black cross.

2.2. Data Processing

The data were processed using the standard HIFI pipeline in HIPE 4.10 (Ott 2010), then exported into FITS format for further analysis using the IRAM Gildas software package (http://www.iram.fr/IRAMFR/GILDAS). The HIPE task FitHiFiFringe was used as part of the pipeline processing to remove standing waves from the data. This was followed by the task DoDeconvolution which utilized the multiple local oscillator settings to extract single-sideband spectra. In Figure 3, we show data for a limited range of velocities around the frequency expected for each of the lines. The continuum as well as the wings of nearby strong spectral lines have been removed by baseline fitting. A broader view of these extremely sensitive submillimeter spectra will be presented elsewhere.

The two orthogonal linear polarizations of each of the HIFI bands are received by separate feed horns and processed independently. They thus inevitably have slight relative pointing offset on the sky, which due to the complex nature of the Orion

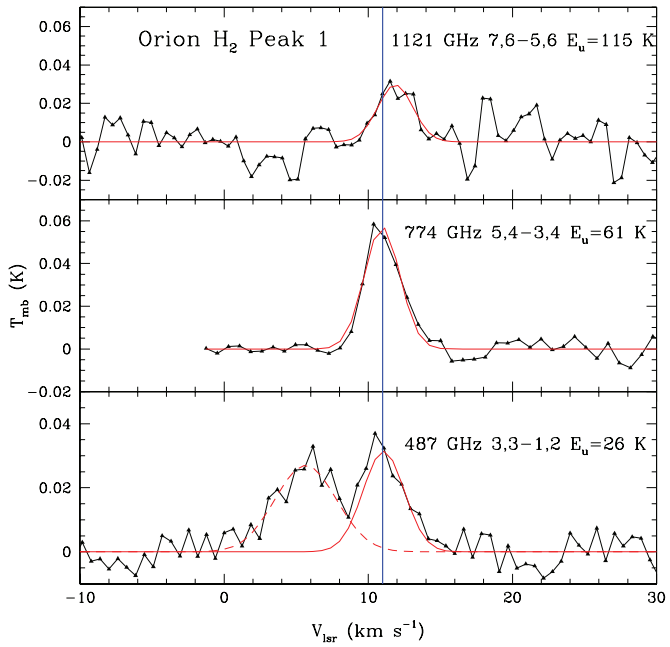

Figure 3. Spectra of the three rotational transitions of O_2 observed with the *Herschel* HIFI instrument toward the Orion H_2 Peak 1 position. The intensity scale is the main beam brightness temperature (antenna temperature divided by main beam efficiency). The red solid lines are fitted Gaussians, which all peak at LSR velocities between 11 and 12 km s^{-1}. For the 487 GHz transition there is clearly a second feature, indicated by the broken red line, which we attribute primarily to O_2 emission from the Hot Core at $v_{lsr} = 5.5$ km s^{-1}, as discussed in the text.

Table 1
Parameters of Observed O_2 Lines

Transition	Frequency (GHz)	$\int T_{mb} dv$ (K km s^{-1})	V_0 (km s^{-1})	ΔV (FWHM) (km s^{-1})	T_{mb} (peak) (K)
3, 3–1, 2	487.249	0.095 ± 0.011	10.96 ± 0.16	3.05 ± 0.40	0.029
		0.113 ± 0.013	5.70 ± 0.23	4.43 ± 0.65	0.024
5, 4–3, 4	773.840	0.177 ± 0.008	10.96 ± 0.07	2.91 ± 0.16	0.057
7, 6–5, 6	1120.715	0.091 ± 0.018	11.87 ± 0.29	2.87 ± 0.62	0.030

region gives us useful information on the source location, which is discussed in Section 3.3.

We see that there is a feature for each transition that peaks between 11 and 12 km s^{-1} (all velocities refer to the Galactic local standard of rest). The results from fitting a single Gaussian to each of these features are given in Table 1. The presence of numerous other lines especially close to the 487 GHz O_2 line means that the uncertainties in the line parameters are increased by the uncertainties in the fitted baselines. For the lowest-frequency transition, this may well be the dominant contribution to the total error, so that the uncertainties given in Table 1 must be regarded as conservative. The 487 GHz transition shows a second component near 5 km s^{-1}, which is a separate entry in Table 1. We attribute this feature primarily to O_2 emission from the Hot Core being picked up only in the large beam at this relatively low frequency. This is the only transition in which there is evidence for this second velocity component. The issue of the O_2 signal coming from the Hot Core, as well as other possible contributions, is discussed further below.

3. IDENTIFICATION AS MOLECULAR OXYGEN

Given that the integrated intensities represent 8.5σ, 22σ, and 5σ statistical features, there is little doubt that we have detected emission lines at the frequencies of each of the three O_2 transitions that we have observed at the H_2 Peak 1 position. The question of whether the features are due to molecular oxygen depends on the agreement and plausibility of the velocities, the consistency of the line intensity ratios, and the presence or absence of other carriers at the three frequencies.

The $\simeq$11 km s^{-1} component of the 487 GHz transition and the two higher-frequency transitions are all consistent in terms of line width. The central velocity of the 1121 GHz line is higher by about 0.9 km s^{-1} than the central velocities of the other two lines. The formal uncertainty on the fitted central velocity is 0.3 km s^{-1}, and the difference in velocities is thus three times this, although less than 1/3 of the FWHM line width. It is thus possible that, assuming all three lines are from O_2, the velocities are in agreement but we are seeing a statistical fluctuation in the fitting of the central velocity, most likely of the highest-frequency line. Alternatively, the highest-frequency line is sampling different gas.

3.1. Interloping Lines

It seems improbable that a single molecular species other than O_2 would have three spectral lines that match so closely with those from the species of interest. It is more plausible that the three spectral features in question are produced by three different "interloper" molecules, but in this case they additionally must have essentially identical line widths. While we cannot rule out this possibility, it should be born in mind that in this region of Orion, there is a wide variety of line shapes and widths due to the presence of multiple kinematic structures, so the species responsible would have all to share one specific set of line profiles and widths, further reducing the likelihood of this explanation.

We have carried out a targeted analysis to assess likelihood that the observed spectral features are due to known molecular species. To do this, we first selected all molecular transitions found in the SPLATALOGUE catalog (http://www.splatalogue.net) falling within 5 km s^{-1} of any of the three O_2 lines observed, and having upper state energies less than 1000 K. There were two species (CH_3NH_2 and CH_3OCHO) having lines possibly interfering with the 487 GHz O_2 line, three species ($(CH_3)_2CO$, g-CH_3CH_2OH, and $OS^{18}O$) close to the 774 GHz line, and six species ($CH_3{}^{13}CH_2CN$, g-CH_3CH_2OH, HCCCHO, CH_3NH_2, g-C_5H, and t-CH_2CHCHO) proximate to the 1121 GHz line.

For each species, we used the CASSIS program (http://cassis.cesr.fr) to simulate the emission spectrum for a 5″ diameter source having line width between 2 km s^{-1} and 4 km s^{-1}, assuming LTE with kinetic temperatures between 75 K and 150 K. In every case except one (discussed below) we found that we had sufficient frequency coverage to include undetected stronger lines located somewhere in the HIFI spectrum. From the nondetections, we could set an upper limit to the column density of the species in question that was so low that all lines in the vicinity of the O_2 transitions were significantly weaker than the observed O_2 main beam brightness temperatures. The range of frequency covered in the HIFI spectra ensured that transitions from states of comparable energy above the ground state to those producing possibly interfering lines were observed. Thus, the gas temperature could not be adjusted in a manner to make the lines close to O_2 relatively more intense than transitions of other carriers that were not detected. An example of this is $(CH_3)_2CO$ (acetone). This molecule has a transition only 12 MHz from the 773.8397 GHz O_2 line, but

also has a group of transitions near 774.4 GHz predicted to be an order of magnitude more intense than the line close to O_2. We do not detect the higher-frequency lines. The sensitivity of our data is such that the possible contribution to the O_2 line is more than an order of magnitude smaller than the observed feature. In this manner, we were able to eliminate 11 out of the total of 12 potentially interfering molecular species from consideration.

One problematic species is CH_3OCHO (methyl formate), whose $40_{6,34}$–$39_{6,33}$ transition in the $v = 1$ state of the E species has rest frequency 487251.99996 MHz, compared to 487249.3755 MHz for the 3, 1–3, 2 O_2 transition. This is the only O_2 transition with possible interference from this species. The upper level energy is 705 K. A number of narrow features in the full HIFI spectrum are reproduced assuming that methyl formate is present emitting with a centroid velocity of 8 km s^{-1} and a line width of 2.5 km s^{-1}. If we assume that we are directly pointed at a 5″ source having kinetic temperature 100 K, we derive a column density of 1.5×10^{17} cm^{-2}. The exact value of the column density depends on the location and characteristics of the source relative to the HIFI beams, as well as the complex characteristics of emission from this species found by Favre et al. (2011). If the emission is entirely from the MF4 source (see Figure 2), the column density required would be considerably greater than found by Favre et al. (2011) so there may well be an extended emission component contributing. With these values defining the methyl formate emission, a significant portion of the 5.5 km s^{-1} feature of the 487 GHz O_2 line seen in Figure 3 could be due to this species. Note that to reproduce the 11 km s^{-1} O_2 feature, the CH_3OCHO would have to be at 12.6 km s^{-1}, a value that is outside the range found by Favre et al. (2011), seen in our *Herschel* data, or found for any of the other species in this region of Orion.

The 5.5 km s^{-1} feature seen in the 487 GHz O_2 transition in the bottom panel of Figure 3 is at the velocity observed for most emission from the Hot Core region near KL. If all or part of this feature is due to O_2, the fact that we see it only in the 487 GHz spectrum is not likely to be a result of excitation; as discussed at length in Section 4.1, the O_2 transitions are likely to be close to thermalization and the relative intensity of the 774 GHz line compared to that of the 487 GHz line will not be very different from unity. We are more likely seeing a result of the very different beam sizes and the offset between the Hot Core and H_2 Peak 1. The angular offset is 27″ and the 1/*e* beam radii are 26.″3, 16.″6, and 11.″4, at 487, 774, and 1121 GHz, respectively, yielding coupling factors to a point source 0.34, 0.07, and 0.003, respectively. The finite size of the Hot Core will modify these results slightly, but it is still the case that when pointed at H_2 Peak 1, the 487 GHz beam will couple moderately well to the Hot Core, but the two higher-frequency beams will have very small coupling, explaining why the 5.5 km s^{-1} feature is seen only in the lowest-frequency O_2 line. This issue is discussed further in Section 5.

Another aspect of the confirmation that the three lines shown in Figure 3 are indeed produced by O_2 is the "chemical poverty" of the H_2 Peak 1 position relative to that of KL and the Hot Core. This is illustrated by comparing the two spectra in Figure 4, which shows a dramatic reduction in the strength of almost all lines at H_2 Peak 1 compared to KL. Many species drop by more than an order of magnitude in integrated intensity. The line crowding in Orion KL is one of the reasons we chose to avoid this source in our initial observations of O_2 with HIFI. A small number of features are stronger, or at least more readily visible at H_2 Peak 1. At this point, we have not been able to make

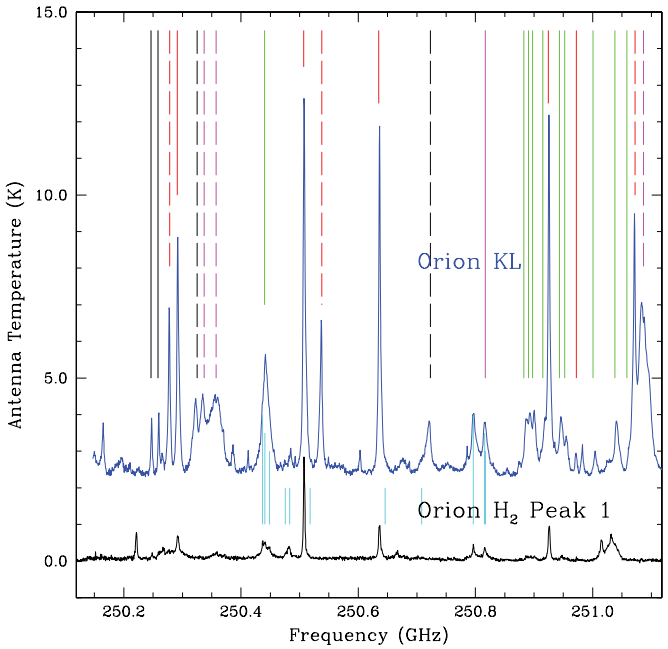

Figure 4. Spectra taken at the CSO in 2011 January, while observing the NO molecule. The upper spectrum is of KL, while the lower spectrum is of H_2 Peak 1. The components of the $J = 5/2$ to $J = 3/2$ transition of NO are indicated by cyan lines, transitions of CH_3OH by red lines, of C_2H_5CN by green lines, of SO_2 and $^{34}SO_2$ by magenta lines, of NS by black lines, and of CH_3OCHO by black lines. Identifications of transitions in the signal sideband are indicated by solid lines and of transitions in the image sideband by dashed lines. The source velocity has been assumed to be 9 km s^{-1}, so that transitions from the Hot Core, typically having velocities 5 km s^{-1} to 6 km s^{-1}, are slightly shifted from their identifying lines.

secure identification of most of these. The conclusion is that finding an "interloping species" mimicking the three putative O_2 lines in Figure 3 is definitely much less likely at H_2 Peak 1 than it would be at Orion KL.

3.2. O_2 Line Velocities and Source Identification

Studies of the central portion of the Orion Molecular Cloud in different molecular tracers have resulted in a number of compact regions being associated with the velocity range 10–12 km s^{-1}, despite this being quite distinct from the nominal velocity of the Hot Core (5–6 km s^{-1}) and of the Compact Ridge including KL itself (8–10 km s^{-1}). In what follows, we briefly discuss these sources, with our goal being to show that associating the observed velocity range of the O_2 lines with one of these regions is not unreasonable.

Pauls et al. (1983) identified a source which they denoted "Peak A" in NH_3 (3, 3) emission, at location $\alpha_{B1950} = 5^h32^m46.^s7$, δ_{B1950} –05°24′24″. Although the centroid velocity of this source is 2 km s^{-1}, the centroid of the spectrum at offset position (−2″, 2″), thus displaced toward our H_2 Peak 1 position, is ≃10 km s^{-1}. Wilson et al. (2000) discuss a 10–12 km s^{-1} component of the (4,4) transition of NH_3. These authors provide little information about its location, but it is apparently the northwest portion of the Hot Core and could be an extension of Peak A. As such it is likely within 5″ of the Hot Core nominal position, offset by ≃27″ from our H_2 Peak 1 position. Plambeck & Wright (1987) see a relatively distinct peak in HDO in a velocity bin spanning 10.5–15.5 km s^{-1} at a position coincident with Peak A, which is 8″ to the northwest of the Hot Core, and thus about 21″ from H_2 Peak 1. Masson & Mundy (1988) present a marginally spectrally distinct feature in the 12–14 km s^{-1} range in HC_3N

Table 2
Parameters of the Observed $C^{17}O$ $J = 7$–6 Line at H_2 Peak 1

Component	$\int T_{mb} dv$ (K km s^{-1})	V_0 (km s^{-1})	ΔV (FWHM) (km s^{-1})	T_{mb} (peak) (K)
1	9.00	3.22	27.0	0.31
2	11.40	9.36	13.1	0.82
3	8.72	9.21	4.3	1.90
4	0.88	10.33	1.4	0.59

$J = 12$–11, in the overall spectrum of the Hot Core, and find that emission at around 13 km s^{-1} peaks in the "Western Clump" which is $\simeq 5''$ west of IRc2, and essentially coincident with Peak A. However, the velocity range 9.5 km s^{-1} to 11.5 km s^{-1} is also characteristic of the northern ridge cloud, observed in a number of species by Wright et al. (1996).

Murata et al. (1991) carried out a study of CS $J = 2$–1 and $J = 3$–2, and found a number of interesting structures, including numerous clumps which are quite prominent in the velocity range 9.9–11.4 km s^{-1} in their interferometric map of the higher-frequency line. Most of these lie along a northeast–southwest line defining the Compact Ridge, but there are three additional (unnumbered) peaks. The first is just $2''$ southeast of H_2 Peak 1, the second is about $16''$ south of our pointing position, and the third is $7\farcs5$ east and $20\farcs6$ south of our H_2 Peak 1 position. This last peak is coincident with the Western Clump–Peak A feature. While no details are given about these peaks, they seem to be part of an arc-shaped ring of emission that lies just outside the blue lobe of the CO bipolar outflow mapped by Erickson et al. (1982). Murata et al. (1992) reported 3 mm continuum mapping of the central portion of Orion, in which a number of condensations were identified. Of greatest relevance to the present study is the "Cnt A" peak which coincides with the second CS peak of Murata et al. (1991), and "Cnt D," which is coincident with the third CS peak, and thus with Western Clump–Peak A.

A recent high-angular resolution study of methyl formate (CH_3OCHO) by Favre et al. (2011) indicates that at least two small clumps have a second kinematic component at velocities higher than the 7 km s^{-1} to 8 km s^{-1} characteristic of most of the emission in the center of the Orion molecular cloud surrounding the Hot Core and the Compact Ridge. One of these clumps, denoted MF4, has its second velocity component, in the three different methyl formate lines observed, at between 10.2 and 11.4 km s^{-1}, thus quite similar to the velocities of the O_2 lines. This condensation agrees in position with the Western Clump–Peak A feature, confirming that this velocity range does seem to be characteristic of this compact source. The issue of the identification of a specific condensation with the O_2 emission will be discussed further in what follows and in Section 6.

One line observed with *Herschel* HIFI simultaneously with the 774 GHz O_2 line is the $J = 7$–6 transition of $C^{17}O$. A hint of a peak at velocity greater than 10 km s^{-1} can be seen in the ^{12}CO $J = 7$–6 line observed by Pardo et al. (2005), but in the vicinity of KL the profiles are dominated by the broad wings of the outflow. In Figure 5, we show the spectrum of the line of the rare isotopologue observed with *Herschel* HIFI. The asymmetry in the narrow component of the emission is immediately apparent, and we also show a four-Gaussian component fit, which is the minimum required to reproduce the observed line profile reasonably well. We give the parameters of the components in Table 2. The presence of the wide component and the asymmetric narrow component leaves the uniqueness of

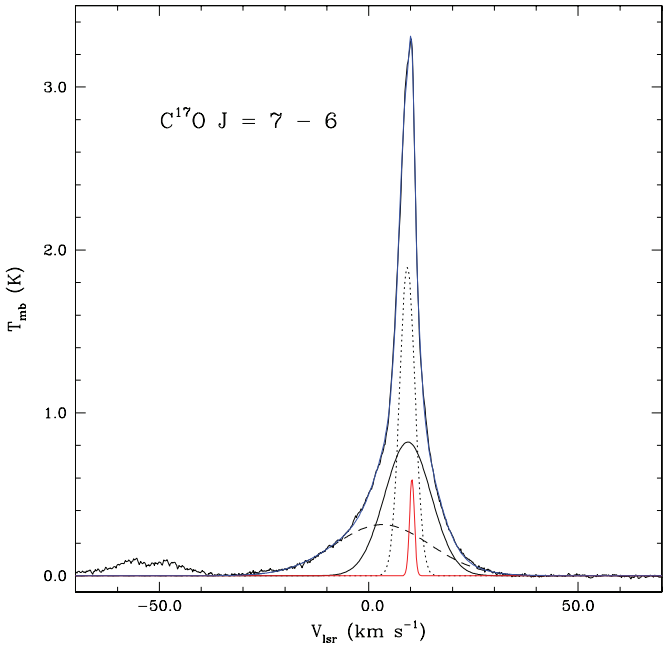

Figure 5. Spectrum of $C^{17}O$ $J = 7$–6 emission at the H_2 Peak 1 position obtained simultaneously with the O_2 774 GHz data using *Herschel* HIFI. The four-Gaussian fit indicates a pedestal feature $\simeq 22$ km s^{-1} wide (long-dashed curve) and three narrower components. The narrowest of these components peaks at a velocity of 10.3 km s^{-1}.

(A color version of this figure is available in the online journal.)

the very narrow component uncertain. It is clear, however, that there must be a component of the gas having central velocity in excess of 10 km s^{-1} at the H_2 Peak 1 position. In Section 4.3, we use the $C^{17}O$ emission to determine the column density of H_2 and the fractional abundance of O_2.

Another relevant molecule is NO, which can be produced by reaction of atomic nitrogen with OH, analogous to the pathway for producing O_2. We have observed the complete set of the fine- and hyperfine-structure components of the $^2\Pi_{1/2}$ $J = 5/2 \rightarrow 3/2$ transition, which fall between 249.6 and 251.6 GHz, with the Caltech Submillimeter Observatory (CSO) in 2011 January. The beam size was $32''$ FWHM and the beam efficiency was 0.73. The full spectrum is shown in Figure 4. We have focused on the relatively unblended and unconfused trio of hyperfine components near 250.8 GHz, and used CLASS software to fit the spectrum based on optically thin relative line intensities and two line components. The parameters for the wide component are $v_0 = 9.3$ km s^{-1}, $\Delta v_{FWHM} = 19.0$ km s^{-1}, and for the narrow component, $v_0 = 10.4$ km s^{-1}, and $\Delta v_{FWHM} = 3.1$ km s^{-1}. The data and the best-fit profile with these two components are shown in Figure 6. The excellent fit confirms that there is a component having centroid velocity and line width quite different from those characteristic of the Hot Core or the region around KL, and which are close to the parameters of the O_2 lines.

The integrated intensity in the narrow component of the NO 250.796 GHz line is $\int T_{MB} dv = 1.4$ K km s^{-1}. Non-LTE models of NO were carried out using the RADEX code and collision rates from Lique et al. (2009b). They indicate beam-averaged column densities of 2.7×10^{15} and 1.45×10^{15} cm^{-2} for $n(H_2) = 5 \times 10^5$ cm^{-3}, $T_k = 77.5$ K, and 10^4 cm^{-3}, 100 K, respectively. The corresponding column densities of O_2 in a non-LTE treatment are 6.5 and 7.5 $\times 10^{16}$ cm^{-2}, respectively. Apparent beam-averaged abundance ratios $NO/O_2 = 0.04$ and

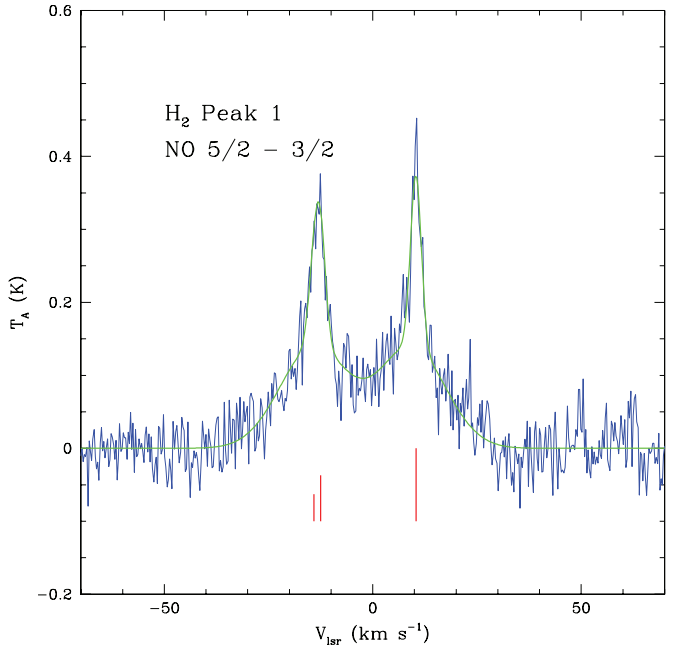

Figure 6. Spectrum of the $F = 7/2$–$5/2$, $F = 5/2$–$3/2$, and $F = 3/2$–$3/2$ hyperfine components of the $J = 5/2$–$3/2$ transition of NO. The relative intensities and offsets referenced to the best-fit velocity of 10.4 km s^{-1} for the low dispersion portion of the strongest $F = 7/2$–$5/2$ hyperfine component are indicated by the vertical lines. The combined best-fit spectrum of the two kinematic components for each of the three hyperfine components is indicated by the solid green curve.

(A color version of this figure is available in the online journal.)

0.02 are deduced. The excitation of NO is more sensitive to density and temperature than that of O_2. Observations of higher transitions of NO will help to constrain the conditions in the O_2-emitting region and ultimately could help determine the ratio of atomic nitrogen and oxygen in the gas phase.

HIFI observations of the 620.710 GHz 5_{32}–4_{41} transition of ortho-H_2O in Orion have yielded, in addition to a broad thermal emission feature seen throughout the central portion of the cloud, a very narrow feature close to 12 km s^{-1}(G. J. Melnick et al. 2011, in preparation). This has many characteristics of maser emission, with extremely narrow line widths $\leqslant$1 km s^{-1}. The size of the narrow-line emission region is difficult to determine due to the presence of large gradients in the thermal emission, but the source location is likely coincident with or slightly north of the H_2 Peak 1 position. Populating the upper level of this transition more than 730 K above the ground state (as well as the location of the emission) is more consistent with spatially extended shocked gas than with any of the compact sources discussed above.

3.3. Constraints on Source Location From Pointing Offsets

The two linear polarizations (H and V) observed by HIFI have a small relative pointing offset, which is different for each band. There are clear detections in each polarization of the 774 GHz O_2 transition each of two well-separated observing epochs (2010 March and September). The 1121 GHz line lacks sufficient signal-to-noise ratio to allow epoch- and polarization-dependent analysis, and the 487 GHz transition has a much larger beam and marginal signal-to-noise ratio.

When processed through HIPE version 5, the pointing offsets of the polarizations relative to the nominal pointing direction are recorded. For March, the α and δ offsets for H and V are

Table 3
Parameters of the Broad Component of the $C^{17}O$ Line

Epoch	$\int T_{\rm mb} dv$ (K km s^{-1})	$\sigma[\int T_{\rm mb} dv]$ (K km s^{-1})
H(Mar)	9.54	0.15
V(Mar)	13.47	0.37
H(Sept)	22.17	0.18
V(Sept)	12.51	0.13

(−0.″9, +2.″1) and (+0.″9, −2.″1), while for September they are (+0.″5, −2.″2) and (−0.″5, +2.″2), respectively. Thus, the offsets from separate polarizations have almost been exactly interchanged due to the six months that have elapsed between the two sets of observations.

The V(March) and H(September) pointing direction is in a direction offset toward the Hot Core by 2.″3, and the V(September) and H(March) data are offset in the opposite direction by an equal amount. We can investigate whether the measured intensities are consistent with a source for the O_2 emission located at the position of the Hot Core. To do this, it is thus reasonable to average together the H data from September with the V data from March, and the V data from September with the H data from March. Doing this we find $\langle \int T[\mathrm{H(Sept)} + \mathrm{V(Mar)}] dv \rangle = 0.160 \pm 0.023$ K kms^{-1}and $\langle \int T[\mathrm{V(Sept)} + \mathrm{H(Mar)}] dv \rangle = 0.210 \pm 0.012$ K kms^{-1}. The ratio of the integrated intensities is $\langle \int T[\mathrm{V(Sept), H(Mar)}] dv \rangle / \langle \int T[\mathrm{H(Sept), V(Mar)}] dv \rangle = 1.31 \pm 0.20$.

The Hot Core is separated from the H_2 Peak 1 nominal pointing position by 24.″6. Adding the offsets for the different epochs appropriately, we find that the distance for the H(Sept) and V(Mar) data is 22.″4, and for the V(Sept) and H(Mar) data is 26.″9. Taking the Hot Core source to be small compared to the antenna beam size, the ratio of the signal measured when pointing closer to the source to that found when pointing farther from the source is given by $\exp((d_{\rm farther}/\theta_0)^2 - (d_{\rm closer}/\theta_0)^2)$, where θ_0 is the $1/e$ radius of the beam, equal to 16.″6 at 774 GHz. The resulting ratio is 2.27.

Relevant information about pointing and source location is provided by the other lines observed simultaneously with the O_2. We see changes in most lines, and the $C^{17}O$ line is particularly useful as it is relatively isolated as well as quite strong. It seems reasonable that the broad component of this line originates in a relatively small region near the Hot Core. Table 3 includes the data for the two polarizations at two epochs. The strength of the broad component is sufficient that we find ratios of the integrated intensities (as defined above) V(Mar)/H(Mar) = 1.41 and H(Sept)/V(Sept) = 1.77, with an average value equal to 1.59. Both ratios are in the sense expected for a point source in the vicinity of the Hot Core, and "flip" in the manner that is expected.

The formal statistical error for each ratio above is less than 4%, so these two measurements are marginally consistent with their average value. However, the data in Table 3 suggest that there is another systematic difference, which can be seen in the average of H and V in September being significantly greater than the average of H and V in March by a factor of 1.5. Since the relative pointing offsets of the two polarizations are essentially just interchanged between the two observing epochs, this suggests that there was an overall pointing change between the periods in which the observations were carried out.

Assuming we are observing a point-like source at the nominal distance of the Hot Core, we can solve for the pointing offset, which is 2.″4 in the sense that the average pointing direction in September was this amount closer to the position of the Hot Core than in March. Although this error results in a large difference in the signal received when observing a source on the "side" of the beam, this is a relatively small pointing error (≃FWHM/12), which is within the expected pointing precision for *Herschel* (Pilbratt et al. 2010). Our data are only marginally consistent with the O_2 emission being a small source at the location of the Hot Core. The NH_3 emission from the northwest portion of the Hot Core, the Peak A–Western Clump, and the Murata et al. (1991) CS clumps are all somewhat closer, and thus more consistent with our measurements.

4. ANALYSIS

4.1. Collisional Excitation of O_2

Since the millimeter- and submillimeter-wavelength transitions of O_2 are magnetic dipole transitions, their spontaneous decay rates are relatively small. Thus, in the relatively dense regions being observed, it is likely that collisions are the dominant excitation mechanism. Orlikowski (1985) carried out calculations for collisions between O_2 and He atoms (as surrogates for H_2 in $J = 0$ level) for levels defined by rotational quantum numbers $N = 1$ and 3, at a total energy of 300 cm^{-1} (corresponding to 432 K). Corey et al. (1986) performed similar calculations for excitation from $N = 1$ and 3 to $N = 3$, 5, and 7 levels for a collision energy of 313 K. The results suggest a propensity for collisions in which the quantum number F, which is equal to $N-J$ (and hence $= -1$, 0, or +1), does not change. Bergman (1995) and Valkenberg (1995) carried out close-coupled calculations of O_2 by He over a range of temperatures relevant for interstellar clouds, using a semi-empirical interaction potential and a number of approximations.

The uncertainty due to the potential energy surface (PES) has been reduced by the use of an improved surface in the recent close-coupled calculations by Lique (2010). The recent study finds that the collisions in which F is unchanged have rate coefficients $\simeq 10^{-10}$ cm^3 s^{-1}, essentially independent of N. The collisions in which N changes are a factor of 10 smaller for low N, and almost a factor of 100 smaller for $N \geqslant 10$. The transitions with the largest cross sections do not correspond to ones for which radiative transitions are allowed. Thus, the upper level of an observed transition is generally not populated by a collision from the lower level of the transition. The result is that a critical density defined in terms of the spontaneous decay rate divided by the deexcitation rate coefficient (for the same levels) is overestimated.

Given that we expect the transitions observed to be optically thin, the most meaningful quantity is simply the fractional population of the upper level, since the observed antenna temperature is directly proportional to this quantity. Using the rate coefficients at a kinetic temperature of 100 K from Lique (2010), scaled by a factor of 1.37 to account approximately for H_2 rather than He as a collision partner, we find that the upper level fractional populations are within 10% of their LTE values for densities above 1×10^3 cm^{-3} for the 487 GHz transition, 1.3×10^4 cm^{-3} for the 774 GHz transition, and 2×10^4 cm^{-3} for the 1121 GHz transition. This density for the 1121 GHz transition is a factor of six smaller than the critical density defined in the usual manner.

In moderate density interstellar clouds, the molecular hydrogen density is $n(H_2) \simeq 10^3$ cm^{-3}, which is sufficient to bring only the population of the (3, 3) level close to LTE; the populations of the upper levels of higher-frequency transitions will be subthermal. However, in regions such as the centers of giant molecular clouds, where densities are generally $\geqslant 10^5$ cm^{-3} and certainly in excess of 10^4 cm^{-3}, the fractional populations of the upper levels of all transitions will be close to LTE values. This is confirmed by a fully non-LTE treatment of the O_2 excitation, which produces the same result for column density and temperature when the hydrogen density is $\geqslant 10^4$ cm^{-3}. It is thus appropriate to use the relative line intensities with the assumption of LTE to determine the kinetic temperature and the total O_2 column density.

4.2. Temperature of the O_2-emitting Region

We can use the three transitions observed to determine the temperature of the O_2-emitting region. To do this we first assume that the source can be characterized by a single temperature and that it fills the beam of all three transitions observed. Both of these assumptions may only hold approximately. If there is a fractional beam-filling factor less than unity, but which is the same for all beams, it does not affect their relative intensities or the beam-averaged column density that we determine. Assuming that the source does fill the main beam of all three transitions and that the emission is optically thin, the integrated main beam brightness temperature is proportional to the upper level column density of the transition observed, N_u, through the relationship

$$N_u(\mathrm{cm}^{-2}) = 1.94 \times 10^3 \frac{\nu^2(\mathrm{GHz})}{A_{ul}(s^{-1})} \int T_{\mathrm{mb}} dv \,(\mathrm{K\,km\,s^{-1}}), \quad (1)$$

where ν is the frequency of the transition and A_{ul} is its spontaneous decay rate. Assuming LTE, as discussed above, the ratio of the column densities of two transitions is determined only by the kinetic temperature of the gas. With three transitions, we can form two such ratios, and from each determine the range of kinetic temperatures consistent with the observations (including at least statistical uncertainties in $\int T_{\mathrm{mb}} dv$). The results are shown in Figure 7. The data in Table 1 yield $0.45 \leqslant I(487)/I(774) \leqslant 0.63$ and $0.40 \leqslant I(1121)/I(774) \leqslant 0.65$. These limits define the temperature limits shown in Figure 7. A kinetic temperature between 80 K and 100 K seems most likely, but values between 65 K and 120 K are consistent with the relative intensities of all three transitions observed.

From Equation (1), we obtain $N(5, 4) = 4.5 \pm 0.21 \times 10^{15}$ cm^{-2}. With the kinetic temperature defined consistently by the two ratios of the three integrated intensities, the total O_2 column density relative to that in $(N, J) = (5, 4)$ can reliably be calculated, and the result is shown in Figure 7. The energy of the $(N, J) = 5,4$ level is such that there is remarkably little variation in the fraction of the total O_2 in this one level. We combine the uncertainty in $N(5, 4)$ with that in the kinetic temperature to determine the beam-averaged column density $N(O_2) = 6.5 \pm 1.0 \times 10^{16}$ cm^{-2}.

4.3. Filled-beam Fractional Abundance of O_2

Due to the wide range of temperatures and kinematic variations in the gas toward H_2 Peak 1, it is difficult to determine the H_2 column density to compare with that of the O_2 observed. The $C^{17}O$ $J = 7$–6 transition discussed in Section 3.2 is a good

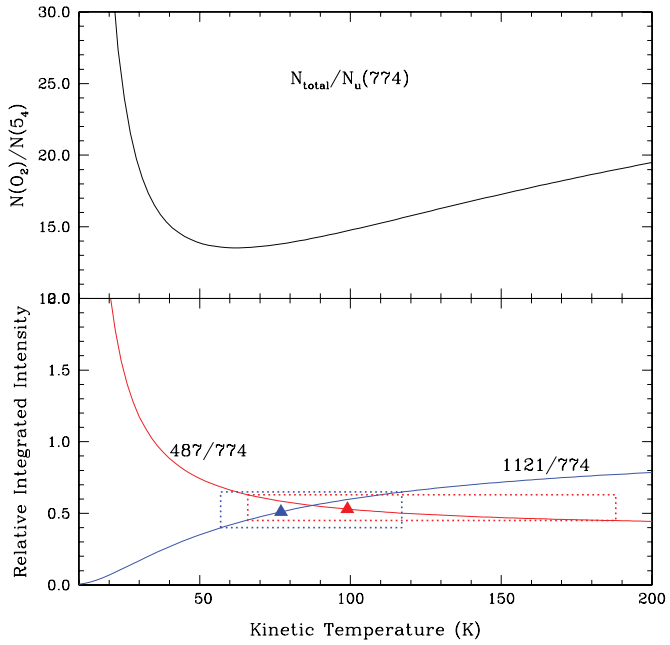

Figure 7. Lower panel: intensity of the 487 GHz O_2 transition relative to the 774 GHz transition, and of the 1121 GHz transition relative to the 774 GHz transition. These values assume that the beam-filling factor is the same for the three transitions and that all levels are populated according to LTE. The triangles are from the results given in Table 1. The dotted boxes are defined by the statistical uncertainties in the observed intensity ratios, and the corresponding values of kinetic temperature that are implied. Upper panel: total column density of O_2 relative to that in the upper level of the 774 GHz transition, $(N, J) = (5, 4)$. In LTE, this depends only on the kinetic temperature as shown here.

(A color version of this figure is available in the online journal.)

candidate for this, since it is optically thin, and at these elevated temperatures, depletion of carbon monoxide should not be significant. The width of this line is sufficient to include all hyperfine components, but as discussed in Section 3.2, we do see three velocity components in addition to the very wide component, presumably associated with the molecular outflow. A four-Gaussian fit is very satisfactory and yields the results given in Table 2. While the velocity of component 4 (10.3 km s^{-1}) agrees best with that of the O_2, the line width (1.3 km s^{-1}) is considerably narrower than the $\simeq$3 km s^{-1} measured for the three O_2 lines (Table 1), so it is difficult to make a definitive correspondence.

Using Equation (1), we find $J = 7$ $C^{17}O$ column densities 3.3×10^{13} cm^{-2} for the 10.3 km s^{-1} component and 7.8×10^{14} cm^{-2} for the combination of the three narrow components (2–4). If we consider the emission at velocities above 10 km s^{-1} excluding the broad components 1 and 2, we obtain a column density equal to 2.5×10^{14} cm^{-2}. The fraction of $C^{17}O$ in $J = 7$ becomes almost independent of temperature for $T \geqslant 80$ K (varying from 1/13 at 80 K to a minimum of 1/10 at 150 K, and increasing very slightly higher at temperatures below 300 K). We adopt a value of 1/11, which yields $N(C^{17}O)$ summed over all levels equal to 3.6×10^{14} cm^{-2} for the very narrow component and 8.7×10^{15} cm^{-2} for the narrow components combined. We take the ratio $CO/C^{17}O = 2460$ (Penzias 1981), and $H_2/CO = 10^4$, yielding $N(H_2) = 8.9 \times 10^{21}$ cm^{-2}, 6.7×10^{22} cm^{-2}, and 2.1×10^{23} cm^{-2}, for the 10.3 km s^{-1} feature, the $\geqslant$10 km s^{-1} emission, and for the combined narrow components, respectively.

This range of column densities corresponds to a range of densities averaged over the projected diameter of the largest *Herschel* beam (44″) of $\langle n(H_2)\rangle = N(H_2)/\theta D = 3 \times 10^4$ to 8×10^5 cm^{-3}. The distance $D = 416$ pc is the weighted mean of four recent parallax measurements of masers in the Orion KL region and of stars in the Orion Nebula Cluster (Hirota et al. 2007; Sandstrom et al. 2007; Menten et al. 2007; Kim et al. 2008). These densities are in harmony with the requirements of the preceding LTE analysis of the O_2 line intensities. With these values bracketing the range of H_2 column density associated with the O_2 emission, we find that the fractional abundance of O_2 is between 3.1×10^{-7} and 7.3×10^{-6}. The higher value is still only $\sim$1% of the total oxygen available. The lower value is comparable to the upper limits found by *SWAS* and *Odin*. If the fractional abundance of carbon monoxide is lower (which is plausible, the adopted value being close to the maximum observed), the column density of H_2 will be increased and the fractional abundance of O_2 proportionately reduced and thus be even smaller compared to the total elemental oxygen abundance.

5. BEAM FILLING AND SOURCE OFFSET EFFECTS

Modeling of the emission for anything but an extended source with a single filling factor for all transitions involves source coupling to beams of the three transitions each having a different beam size. This leads to some effects which we discuss here.

5.1. Effect of Beam Filling

A beam-filling factor less than unity, but which is the same for all transitions, can be produced by an extended but clumpy medium (as suggested by, e.g., the shocked H_2 emission seen in Figure 2). This situation leaves the relative intensities of the transitions unchanged, and thus the temperature we determine for the region responsible for the O_2 emission will be unaffected. The column density of O_2 in the "filled" portion of the beam is increased by the reciprocal of the beam-filling factor. If the O_2 emission is associated with postshock gas traced by H_2 emission, then as shown in Figure 2, the emitting region is extended on the scale of all of the HIFI beams, albeit modestly weaker in the outer portions of the lowest-frequency (487 GHz) beam. The fractional abundance of O_2 may be increased if the tracer of H_2 is uniformly distributed, but may be essentially that derived above if the overall mass distribution is nonuniform, rather than only the distribution of O_2.

If Peak A is the source of the observed O_2 emission, we have to deal with a small source which is also away from the antenna boresight direction. In Appendix B, we discuss the limiting case of an on-boresight source that is so small that it can be considered to be point-like relative to all beams. The ratio of the intensities of two transitions, 2 and 1, can be considered to be the ratio characteristic of the source itself multiplied by the correction factor $R(2/1)$ as defined in Equation (B7) in Appendix B. To derive the required characteristics of the source, we must thus divide the observed ratio by the correction factor. For the ratio of the 1121 GHz transition to the 774 GHz transition, we find

$$\frac{I^{\rm obs}(1121)}{I^{\rm obs}(774)} = \frac{I^{\rm src}(1121)}{I^{\rm src}(774)}\left[\frac{\lambda(774)}{\lambda(1121)}\right]^2 = 2.1\frac{I^{\rm src}(1121)}{I^{\rm src}(774)} \quad . \quad (2)$$

The ratio for the source has to be a factor $\simeq$2 smaller than the observed ratio, which as seen in Figure 7 means a lower kinetic temperature. For an observed ratio of 0.5, a temperature of 70 K is required for a source filling both beams. However, the ratio for a small source must be smaller by a factor of 2.1, and hence equal to 0.24. As seen from Figure 7, this requires a kinetic temperature of $\simeq$35 K.

The second line ratio is again normalized to the intensity of the 774 GHz transition, and hence the correction factor $R(487/774) = [\lambda(774)/\lambda(487)]^2 = 0.4$. As indicated by the appropriate curve in Figure 7, this again corresponds to a lower kinetic temperature for the small source. An observed ratio of 0.5, which requires a filled source temperature of 100 K demands a ratio 2.5 times larger in a small source, and thus a source temperature again $\simeq$30 K. A small source on boresight is consistent with a single temperature determined by the ratios of integrated intensities, but the source temperature is too low given the ease of excitation of O_2 and the temperature of the center of the Orion molecular cloud. It is thus unlikely that the observed O_2 lines are produced by a small source coincident with Orion H_2 Peak 1, but an extended while beam-diluted source can fit the present data.

5.2. Effect of Source Offset

We again restrict our discussion to a small (point-like) source, which when offset by an angle θ produces a signal reduced from that of a source on boresight by a factor which is given by the normalized antenna response pattern:

$$P_n = e^{-(\theta/\theta_0)^2}, \quad (3)$$

where θ_0 ($= 0.601\theta_{\rm FWHM}$) is the $1/e$ beam radius. θ_0 is proportional to the observing wavelength, and so a given offset produces a greater reduction in observed integrated intensity at a higher frequency. Following the discussion of beam filling, we define the integrated main beam temperatures with the source off and on boresight as $I^{\rm off}$ and $I^{\rm on}$, respectively. We then find

$$\frac{I^{\rm off}(1121)}{I^{\rm off}(774)} = \frac{e^{(\theta/\theta_0(774))^2}}{e^{(\theta/\theta_0(1121))^2}} \frac{I^{\rm on}(1121)}{I^{\rm on}(774)}. \quad (4)$$

Since $\theta_0(1121) = 11\farcs4$ and $\theta_0(774) = 16\farcs6$ the correction factor for off-boresight pointing is always less than unity and decreases as the offset increases. To fit a given observed ratio, we require an on-boresight source with a larger ratio, which can only be produced by a higher source temperature. The ratio for the 487 GHz transition to the 774 GHz transition shows the opposite dependence, being greater than unity. Thus, to fit an observed integrated intensity ratio, the off-boresight source would need to have a smaller 487 GHz to 774 GHz ratio than that for an on-axis source, and the effect again is that the source temperature would be greater than if the source were on boresight.

The observed 1121 to 774 ratio, close to 0.5, is what would be produced by an on-boresight small source that if filling both beams would produce a ratio equal to $0.5/2.1 = 0.24$. To obtain an observed 1121 to 774 ratio for a small source off-boresight equal to the intrinsic (filled-beam) source ratio requires that the off-boresight correction be the inverse of the small-source correction, and thus equal to $1/2.1 = 0.48$. This occurs if the source is off axis by just over $13''$.

As seen in Figure 7, the ratio $I^{\rm src}(1121)/I^{\rm src}(774)$ has an upper limit of about 0.8 for a filled source, irrespective of temperature. This would be produced by an on-boresight small source with an (unphysical) ratio of 1.68. However, a *very warm small source off-boresight* could produce the observed ratio of 0.5 with off-boresight correction factor equal to 0.30, which results when the source is off boresight by about $17''$. Especially when the uncertainties are considered, consistent solutions for all three transitions are possible for small sources over a restricted range of offset angles, up to approximately this limit. Since the offset to the Hot Core is close to $27''$, it appears difficult to have this source dominate the O_2 emission we have observed at H_2 Peak 1. One or more of the compact sources discussed previously are more likely the source of the emission. In particular, Peak A (with an offset of $21''$) is consistent with this picture, with gas, and dust temperatures well over 100 K being indicated by other observational data and required to fit the present observations of O_2.

6. DISCUSSION

There seems little reason to doubt that we have detected emission from O_2 but the source of the emission remains imperfectly characterized. The issue at hand is to understand the circumstances that result in the increase in the O_2 abundance from the low levels derived from *SWAS* and *Odin* observations. Two theories for enhanced abundance of O_2, (1) warm dust with restoration of pure gas-phase chemistry and (2) shocks, seem to be relevant possibilities for explaining the present observations. We here give some additional details that bear on explaining our data for H_2 Peak 1 in Orion.

6.1. Warm Dust

It is generally accepted that dust grains in dense clouds without star formation in the immediate vicinity will be sufficiently cold that over time (depending on the density), atomic oxygen will deplete onto grains and to a large degree be hydrogenated to water. In consequence, the grains acquire water ice mantles incorporating a significant fraction of the available oxygen, with an accompanying significant reduction in the gas-phase $X(O_2)$, as developed in the models by Bergin et al. (2000) and Hollenbach et al. (2009) discussed in Section 1. The formation of a massive star in or near the region in question produces radiation that is in a short distance degraded to infrared wavelengths, and which heats dust grains. At modest temperatures, any desorbed O_2 will be returned to the gas, as discussed in Section 1.1. When the grain temperature reaches $\sim$100 K, return of water ice to the gas phase becomes rapid (Fraser et al. 2001). This starts the restoration of "pure" gas-phase oxygen chemistry. The time required to reach steady state depends primarily on the ionization rate, but ultimately a very substantial $X(O_2) \geqslant 10^{-5}$ will be established.

In Figure 8, we show results of a representative calculation, which is based on NAHOON, the Wakelam et al. (2005) model, but using the OSU–1–2009 reaction rate file. The H_2 density is 10^6 cm^{-3}, the gas temperature is 100 K, and grain surface reactions are excluded except for H_2 formation. We assume that at $t = 0$, all of the elemental oxygen that had been on the grain surface is returned to the gas phase, and that the oxygen that had (in the steady-state solution for large times in this model) been in molecular and atomic form, as well as that having been water ice, comes off the grain as H_2O. This reflects the idea that at some point in the past, the grains had been cool enough that all of these species would deplete onto the grain surfaces, and end up as water ice, but the result here is in effect a gas-phase chemistry model. There are also trace oxygen-bearing species such as SO and SO_2 that are in the gas phase at the start of the present calculation, but together they represent less than 0.5% of the total available oxygen.

Starting at $t = 0$, the O_2 fractional abundance builds up steadily, and although initially smaller than that of atomic oxygen soon surpasses it. The two species end up with comparable steady-state abundances (5–7) $\times$ 10^{-5}. The time to achieve

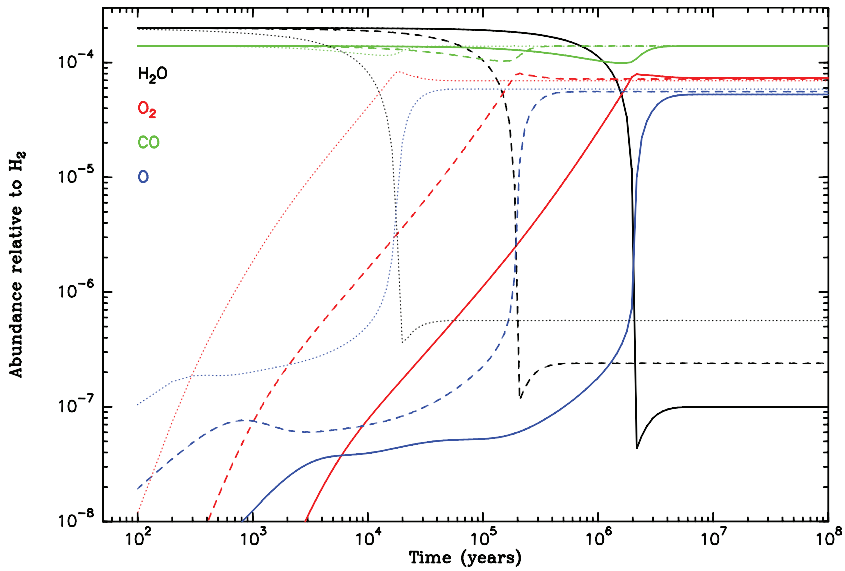

Figure 8. Time evolution of gas-phase abundances of atomic oxygen, molecular oxygen, water, and carbon monoxide in a cloud with dust and gas temperatures equal to 100 K and H_2 density equal to 10^6 cm^{-3}. At $t = 0$, elemental oxygen not in CO is almost entirely in the form of gas-phase water, grain surface water having been returned to the gas phase as a result of the warm grain temperature. The dotted curves are for a cosmic ray ionization rate of 10^{-15} s^{-1}, the dashed curves for 10^{-16} s^{-1}, and the solid curves for 10^{-17} s^{-1}.

maximum abundance of O_2 scales inversely with the cosmic ray ionization rate. The timescales for achieving a given O_2 fractional abundance as well as steady-state abundance are largely independent of the density of the region. The behavior is also largely independent of temperature as long as the dust is warm enough to prevent any significant grain surface depletion to occur. The steady-state fractional abundance of H_2O increases as the ionization rate increases, although the abundances of O and O_2 are only slightly affected.

To evaluate the quantity of gas that may be maintained at conditions for the above chemistry to evolve, we evaluate a highly idealized model based on a single luminous source in a spherically symmetric cloud. Taking a central source with 10^4–10^5 $L_\odot$, plausibly IRc2 (Downes et al. 1981) or else a collection of sources in the region (Gezari et al. 1998) having similar total luminosity, we have carried out a representative calculation of the dust temperature distribution using the DUSTY radiative transfer code (http://www.pa.uky.edu/~moshe/dusty; Nenkova et al. 2000). The center to edge visual extinction is equal to 1000 mag, but this value is unimportant as long as the dust at the cloud edge is cooler than the temperatures of interest. We find that the solutions at distances of interest are quite independent of the radial density distribution assumed to be a power law $n(r) \sim r^{-\alpha}$ with index α between 0 and 2. At the 4×10^{16} cm projected distance of Peak A from IRc2, the dust temperature is 56 K for the lower luminosity and 100 K for the higher. At the 1.5×10^{17} cm projected distance of H_2 Peak 1 from IRc2, the temperatures are 35 K and 55 K, respectively. Thus, even if Peak A is externally heated, the grains will be sufficiently heated to result in "warm dust" chemistry, while those at the distance of H_2 Peak 1 will not.

The fraction of the total opacity between the central source and the location of a particular grain temperature does depend on α. For relatively flat density distributions ($\alpha < 1$), the fraction of the total optical depth is $\leqslant$0.5 for a dust grain temperature of 100 K. While recognizing that this idealized, spherically symmetric model may not be accurate for this complex region, it seems plausible that IRc2 or another source, or the combination of sources in the region can result in warm grains in Peak A, even if this source is not self-luminous. The greater distance to H_2 Peak 1 means that the grains there would still be cold enough to retain significant ice mantles if IR heating were the only operative process warming the dust.

Given that the grains in Peak A may be sufficiently warm that the gas-phase O_2 abundance has been significantly raised, we can examine whether this source is consistent with the O_2 line intensities we have observed. We must thus consider a small-source offset from the beam pointing direction. Following the discussion in Sections 5.1 and 5.2, the 1121/774 ratio is increased by a factor of 2.1 due to small-source size and decreased by a factor of 0.15 due to offset, relative to filled-beam on-boresight model. The resulting correction factor is 0.3, which means that the maximum ratio for a warm beam-filling source of 0.8 becomes 0.25, lower than the observed ratio of 0.51 ± 0.1. For the 487/774 ratio, we get a combined correction factor of 1.12, which when multiplied by the high temperature filled and centered model ratio of 0.45, gives a ratio equal to 0.51, compared to the observed ratio of 0.54 ± 0.1. Considering the uncertainties in source size and geometry, in addition to calibration issues, we conclude that the observed line ratios are consistent with a small warm source located at the position of Peak A.

If Peak A is the source of the 11 km s^{-1} to 12 km s^{-1} emission, the column densities are certainly greater than the filled-beam values given previously. With a representative 10″ for the diameter of Peak A (larger than Murata et al. 1992, as there is some extended emission) and including the attenuation due to being 21″ away from boresight, we obtain a total correction factor of 55 compared to a filled-beam on-boresight source. The $C^{17}O$ used to determine the associated H_2 column density certainly does not all come from this small source, but scaling the H_2 column density implied by the $\geqslant$10 km s^{-1} emission, 6.7×10^{22} cm^{-2}, by the correction factor, we find $N(H_2) = 3.7 \times 10^{24}$ cm^{-2}. The conversion from $C^{17}O$ in $J = 7$ to total $N(C^{17}O)$ is essentially independent of temperature for $T \geqslant$ 100 K. The origin of the O_2 emission in this small region leaves

the emission optically thin, as is the $C^{17}O$ emission for $v \geqslant 10$ km s^{-1}. For a source temperature $\geqslant$150 K compared to the $\sim$100 K value in the filled-beam model, the column density of O_2 will be slightly increased due to the larger partition function (Figure 7). For a temperature of 180 K, we obtain $N(O_2) = 4.6 \times 10^{18}$ cm^{-2} for a 10″ diameter source. The fractional abundance of O_2 is only slightly changed and is equal to 1.3×10^{-6}, a value consistent with the warm grain chemical models. According to the warm dust model as shown in Figure 8, for a low ionization rate of 10^{-17} s^{-1}, the time to reach this fractional abundance is $\leqslant 10^5$ yr.

Murata et al. (1992) derive a mass of 3.2 $M_\odot$ for the Cnt D clump, coincident with the Peak A–Western Clump–MF4 source, as discussed above. Wright et al. (1992) carried out submillimeter dust observations with somewhat lower angular resolution and derived a size of 5″–10″ and a mass of 4–13 $M_\odot$, slightly larger than those of Murata et al. (1992), possibly due to their lower angular resolution. The peak column density from the Murata et al. (1992) data is $N(H_2) = 5 \times 10^{24}$ cm^{-2}, which agrees surprisingly well with that implied by our $C^{17}O$ and related observations keeping in mind that the mass derived from submillimeter dust emission has its own $\sim$factor of three uncertainty. The average density in the clump is $\simeq 2 \times 10^8$ cm^{-3}, which is certainly adequate to thermalize both the O_2 and the $C^{17}O$.

The simplest estimate for the virial mass of this clump, assuming uniform density, and ignoring magnetic fields and external pressure, is $M_{\rm vir} = 5\sigma_{\rm los}^2 R/G$, where $\sigma_{\rm los}$ is the line-of-sight velocity dispersion and R is the cloud radius. The result is $M_{\rm vir} = 8$–19 $M_\odot$, and $M_{\rm vir}/M = 0.7$–4 for the range of sizes and masses determined from the dust emission. This range includes values characteristic of cores in general. While we cannot definitively prove that the observed O_2 lines arise from this compact source, it certainly does seem to be a good candidate to explain our observations.

6.2. Shocks

The H_2 Peak 1 position was selected as it coincides with the strong local maximum in the intensity of the $v = 1$–0 S(1) transition of molecular hydrogen studied by Beckwith et al. (1978). Using several of the vibration–rotation transitions, these authors found an excitation temperature in excess of 2000 K. Since the peak is not in the immediate vicinity of any luminous source, this very high value is a strong indication that this is a result of shock excitation. In the intervening years there has been a plethora of papers that report dramatically improved spatial and spectral resolution (Scoville et al. 1982; Chrysostomou et al. 1997; Schild et al. 1997; Stolovy et al. 1998; Schultz et al. 1999; Salas et al. 1999; Rosenthal et al. 2000; Vannier et al. 2001; Gustafsson et al. 2003; Kristensen et al. 2003; Lacombe et al. 2004; Bally et al. 2011).

Although fluorescence powered by UV radiation from the Trapezium stars dominates the H_2 line emission on degree scales in Orion (Luhman et al. 1994), the emission of highest surface brightness in the molecular core is due mainly to collisional excitation in shocks (Rosenthal et al. 2000). As discussed by these authors, population diagrams based on the wide range of lines available from the Infrared Space Observatory (ISO) clearly indicate a large range of excitation temperatures spanning a few hundred to several thousand K. Multiple shocks are indicated by the pure rotation H_2 transitions observed by Parmar et al. (1994). A relatively low-temperature component is also indicated by the 17 μm $J = 3$–1 rotational transition studied by Burton & Haas (1997). This study also suggested the presence of shocks having velocities as low as 5 km s^{-1}.

High-resolution observations provide evidence of a complex kinematic structure. Among the highest spectral resolution data are those of Chrysostomou et al. (1997) of the H_2 $v = 1$–0 S(1) line, carried out with a velocity resolution of 14 km s^{-1}. These data indicate that the spatially extended H_2 emission peaks at a velocity of 12 km s^{-1} and has an average FWHM line width equal to 37 km s^{-1}, but that localized regions have different central velocities and broader line widths. The highest spatial resolution observations (0.″15; Gustafsson et al. 2003) show complex localized structures having dramatically different central velocities.

The effects of shocks on the abundance of O_2 have been considered in some detail by Bergin et al. (1998); references to reaction rates and earlier studies can be found in that paper. The key point is that the reaction O + H_2 $\rightarrow$ OH + H, which has an activation barrier of 3160 K, can become the dominant production pathway for OH at postshock gas temperatures. This provides a major additional source of OH beyond the primary pathway operative in quiescent clouds in which dissociative recombination of H_3O^+ is the major source of OH. Thus, if there is appreciable preshock atomic oxygen, there will be enhanced production of OH in the shock, which then can react with O via the temperature-independent reaction OH + O $\rightarrow$ O_2 + H discussed in Section 1. FIR observations (Goicoechea et al. 2006) suggest that there is large increase in the abundance of OH as a result of the shock in the Orion KL outflow, but the velocity and line width of the OH do not allow any conclusive association with the O_2 emission.

However, the reaction OH + H_2 $\rightarrow$ H_2O + H, with an activation barrier of 1660 K, competes for the available OH. In addition, there is a back reaction H + O_2 $\rightarrow$ OH + O, which limits the abundance of O_2 if the gas temperature exceeds $\simeq$1000 K and there is some atomic hydrogen present. These conditions are likely to occur following the passage of a strong nondissociative shock. Thus, shocks strong enough to enable production of OH, but in which the postshock temperature does not exceed $\simeq$500 K, result in maximum O_2 production (Bergin et al. 1998). Kaufman (2010) has studied a wide range of nondissociative C-shocks with a wide variety of shock velocities and preshock densities, and finds that maximum O_2 production results from shock velocities 10 km s^{-1} to 12 km s^{-1}, and is relatively independent of preshock gas density. The range of shock velocities over which O_2 column densities in excess of 10^{16} cm^{-2} are produced is broadened for $n(H_2)$ in the preshock gas $\geqslant 10^4$ cm^{-3}. Under optimal conditions, O_2 column densities can be as large as 10^{17} cm^{-2}.

The models of shock chemistry, while still highly idealized relative to the complex structure in the H_2 Peak 1 region (see, e.g., Figure 2), may well produce a relatively large column density of O_2. The conditions required are (1) a C-shock of appropriate velocity, (2) low electron density with $X(e^-) \leqslant 10^{-6}$ to 10^{-7}, (3) sufficiently high preshock density, $n(H_2) \geqslant 10^4$ cm^{-3}, and (4) a significant fraction of available oxygen in gas-phase atomic form. The first three requirements do not seem implausible in this region of Orion, due to the high degree of clumpiness, the high average density, and the wide range of shock velocities present. In considering shock models, we have to allow for a range of shock velocities propagating in a very nonuniform medium. This is to some degree the picture advanced by Salas et al. (1999) in which shocks driven by a stellar wind impinge on (possibly moving) clumps. The

shock velocity in a dense clump will be significantly lower than that in the diffuse interclump medium, and so one can easily imagine a wide range of shock velocities. In addition to the shock propagating into the clump (which may have too low a velocity to produce abundant O_2), there can be a variety of other complex shocks that could release atoms and molecules from the grains, which could subsequently form large amounts of O_2.

The issue of the atomic oxygen abundance is perhaps the most challenging one. For C-shock speeds in excess of $\sim$15 km s^{-1}, the ion–neutral streaming is sufficient to sputter grain mantles and thus produce a large density of atomic oxygen. Even in the absence of sputtering, if the extinction of this region relative for the UV field produced by the Trapezium stars is not greater than $\sim$9 mag, the atomic oxygen fractional abundance could exceed 10^{-5}, which would be sufficient for the C-shock to produce observed column density of O_2. The O_2 column density in the PDR itself ($\leqslant 10^{16}$ cm^{-3}; Hollenbach et al. 2009) is significantly below that observed unless there is some very special geometry involved. Alternatively, a higher-velocity J-shock (such as suggested by the H_2 data) could produce the atomic oxygen. In the dense postshock gas dissociated H_2 reforms quickly. A lower-velocity C-shock propagating into this gas would then produce the O_2 as discussed above. It is also possible that UV radiation generated in the J-shock can, through photoreactions induced in water ice molecules on grains, result in $\simeq$10% of the molecules desorbed being O_2 (Öberg et al. 2009b; K. I. Öberg 2011, private communication), which could be a supplement to the other production channels.

The line profile of the O_2 produced in a shock depends in detail on the geometry, but for the idealized case of a planar low-velocity shock, has a quite narrow-line "core" together with a broad "wing" profile. In order for the line velocity to be shifted from that of the ambient material in the center of Orion by only 3–5 km s^{-1}, the shock direction would have to be close to the plane of the sky. However, if an initially planar shock encounters inhomogeneities, the propagation direction will be modified, and it seems inevitable that some line broadening would result. The observed 11–12 km s^{-1} velocity is shifted relative to the 8–9 km s^{-1} velocity of the ambient gas in the opposite sense of the CO outflow, which has its blueshifted wing extending toward H_2 Peak 1 (Erickson et al. 1982).

A serious problem with the shock model is that while the observed $N(O_2)$, 6×10^{16} cm^{-2}, is $\simeq$ a factor of two less than the maximum $N(O_2)$ that can be produced, the observed column density is a beam-averaged value. Thus, we require the shock to essentially fill a $\simeq 30''$ region, corresponding to $\simeq 2 \times 10^{17}$ cm in size at the 416 pc distance of Orion. Given the highly inhomogeneous structure of the H_2 emission seen in Figure 2, it is difficult to see how our three HIFI beams could be filled with gas that has been through a low-velocity shock all giving projected velocities within a $\pm$1.5 km s^{-1} range. It is possible that the observed emission could be the result of shocks having passed through beam-diluted clumps distributed throughout the beam, thus allowing a reasonable agreement with the relative intensities we have observed. The O_2 column density would, however, have to be higher by the inverse of the beam-filling factor. If this factor were as large as a few, it would put $N(O_2)$ close to the upper limit for shock production of this species.

In summary, while shock models can in principle produce the observed column density of O_2, there are difficulties regarding the initial conditions, particularly the abundance of atomic oxygen, and the observed narrow-line profiles. These can be addressed only by more detailed and extensive modeling.

7. CONCLUSIONS

We have observed three submillimeter rotational transitions of the O_2 molecule in emission, using the HIFI instrument on the *Herschel Space Observatory*. The pointing position was toward Peak 1 of the H_2 emission in Orion. Signals were detected from the 487 GHz, 774 GHz, and 1121 GHz transitions, having peak velocities between 11 km s^{-1} and 12 km s^{-1}, and FWHM line widths $\simeq$3 km s^{-1}. The detection of three transitions and the elimination of the most obvious possible "interloping" lines confirm that the emission is from O_2. The determination of the source of the emission and its characteristics are difficult due to the complexity of the region, but the highlights of the analysis are the following.

1. Assuming that the emission fills the beam at all three frequencies, the relative intensity of the O_2 lines, taken to be optically thin and produced in LTE, suggests that the temperature of the region is between 65 K and 120 K, and that the column density is $N(O_2) = 6.5 \pm 1 \times 10^{16}$ cm^{-2}. Observations of $C^{17}O$ $J = 7$–6 line obtained simultaneously with those of O_2 indicate emission in the same velocity range as observed for O_2. Based on the $C^{17}O$ emission at $v \geqslant 10$ km s^{-1} and assuming $X(CO) = 1 \times 10^{-4}$, we derive an H_2 column density equal to 6.7×10^{22} cm^{-2} and a fractional abundance $X(O_2) \simeq 10^{-6}$.
2. The line centroid velocity is close to that of a number of species in a condensation $\simeq 6''$ west of IRc2, called Peak A, the Western Clump, or MF4 by various authors. Molecules including HDO, HC_3N, NO, and $HCOOCH_3$ have peak emission at velocities between 10 km s^{-1} and 11.4 km s^{-1} toward this condensation, very similar to the observed velocities of the O_2 lines. This is also the Cnt D localized maximum in the dust continuum emission.
3. With only one pointing direction, we do not have definitive information on the exact source of the emission. The position of Peak A is $\simeq 21''$ from the direction of the present observations. The differential pointing of the two HIFI polarizations suggests that Peak A is more likely the source of the emission than the Hot Core, which is farther away from the beam pointing direction.
4. If the $5''$–$10''$ diameter Peak A is the source of the observed O_2 emission, the relative line intensities require that the source be quite warm, with $T \geqslant 180$ K, and the source column density $N(O_2) = 4.6 \times 10^{18}$ cm^{-2}. If the aforementioned $C^{17}O$ emission also originates in this clump, our $C^{17}O$ data imply an H_2 column density equal to 3.7×10^{24} cm^{-2}. This is very similar to the H_2 column density derived from interferometric observations of the dust in this clump, $N(H_2) = 5 \times 10^{24}$ cm^{-2}. The resulting fractional abundance is $X(O_2) = 1.3 \times 10^{-6}$, which is readily obtained in pure gas-phase chemistry.
5. Explanations for the relatively large O_2 fractional abundance compared to the results found by *SWAS* and *Odin* satellites include (1) increase in gas-phase O_2 as a result of warm grains having desorbed water ice mantles with subsequent reestablishment of standard gas-phase chemistry and (2) enhancement of $X(O_2)$ by shocks.
   (1) Heating dust grains to the $\sim$100 K temperature required to desorb water mantles may have resulted from radiative heating, plausibly by nearby luminous sources. In this case, the observed O_2 lines could be emission from Peak A (possibly with contributions from other condensations that are all close enough to IRc2, IRc7, and other heating

sources to have $T_{\rm grain} \geqslant 100$ K). The fractional abundance of O_2 for this model implied by our observations is 1.3×10^{-6}, which is more than an order of magnitude below that achievable. The time required to achieve the observed fractional abundance of O_2 is moderate, $\leqslant$ few $\times 10^5$ yr even for low cosmic ray ionization rate and varying inversely with this rate. Since desorption of water mantles is rapid, the total time for even the first high-mass star to produce a fractional abundance consistent with that observed is compatible with the lifetime of high-mass stars.

(2) A 10 km s^{-1} to 12 km s^{-1} shock can produce the observed O_2 column density only if the emission is not significantly beam diluted. If the shock propagation direction is largely in the plane of the sky, the velocity centroid and line width may be consistent with what is observed. Shocks are generally assumed to be responsible for the widespread H_2 emission observed in this region, but generally taken to have much higher velocities. J-shocks may produce UV radiation that maintains a significant abundance of atomic oxygen. This is required to be present in the gas which is then subjected to lower-velocity shocks which are optimum for producing the observed O_2 column density. Shocks may also explain the water maser emission observed with *Herschel*. In this scenario, the O_2 emission would have to come from numerous clumps distributed throughout the *Herschel* beams, possibly the same condensations responsible for the highly inhomogeneous H_2 emission revealed by high-angular resolution observations.

The O_2 velocities and widths, association with the high-column density warm Peak A source, and the plausibility of the warm dust model suggest that this compact condensation is responsible for the O_2 emission we have observed.

6. The resolution of the origin of enhanced O_2 abundance will require both additional modeling and further observations. Our data do not suggest that the O_2 abundance is sufficiently large to resolve the "oxygen problem," referring to the question of allocating the available oxygen among different forms (grains, ices, O, H_2O, CO, and other molecules; Whittet 2010). Future observations will hopefully yield a more complete understanding of the astrochemistry of O_2 and the distribution of oxygen in dense molecular clouds.

We are indebted to the many people who worked so hard and for so long to make the *Herschel* mission and the HIFI instrument a success. HIFI has been designed and built by a consortium of institutes and university departments from across Europe, Canada, and the US under the leadership of SRON Netherlands Institute for Space Research, Groningen, The Netherlands with major contributions from Germany, France, and the US Consortium members are Canada: CSA, U. Waterloo; France: CESR, LAB, LERMA, IRAM; Germany: KOSMA, MPIfR, MPS; Ireland, NUI Maynooth; Italy: ASI, IFSI-INAF, Arcetri-INAF; Netherlands: SRON, TUD; Poland: CAMK, CBK; Spain: Observatorio Astronómico Nacional (IGN), Centro de Astrobiología (CSIC-INTA); Sweden: Chalmers University of Technology-MC2, RSS, & GARD, Onsala Space Observatory, Swedish National Space Board, Stockholm University-Stockholm Observatory; Switzerland: ETH Zürich, FHNW; USA: Caltech, JPL, NHSC. The O_2 excitation calculations were carried out using the RADEX code (Van der Tak et al. 2007). We appreciate the effort that went into making critical spectroscopic data available through the Jet Propulsion Laboratory Molecular Spectroscopy Data Base (http://spec.jpl.nasa.gov/), the Cologne Database for Molecular Spectroscopy, (http://www.astro.uni-koeln.de/cdms/ and Müller et al. 2001) and the Leiden Atomic and Molecular Database (http://www.strw.leidenuniv.nl/~moldata/ and Schöier et al. 2005). We thank Holger Müller for helpful discussions about molecular spectroscopy. Colin Borys of the NASA Herschel Science Center gave us valuable assistance in unraveling the pointing offsets of the two HIFI polarization beams. We thank Nathaniel Cuningham and John Bally for sending us the FITS image used to make Figure 2. We appreciate the input from John Pearson and Harshal Gupta in terms of useful discussions about molecular structure and astrophysics. Volker Tolls provided valuable information about the WBS noise bandwidth and noise after combining WBS spectral channels. We have benefited from discussions with D. Quan about grain warmup and its impact on molecular cloud chemistry. The Caltech Submillimeter Observatory is supported by the NSF under award AST-0540882. This work was carried out in part at the Jet Propulsion Laboratory, California Institute of Technology, under contract with the National Aeronautics and Space Administration. We thank K. Öberg for helpful information on desorption of molecules from grains, and the referee for a number of valuable suggestions.

APPENDIX A

HIFI RADIOMETER NOISE PERFORMANCE

These relatively long integrations confirm the excellent performance of the HIFI instrument. The noise in all three O_2 spectra is in general quite close to that expected from the radiometer equation. The major limitation on the precision with which this can be determined is the possible presence of very weak spectral lines and of variable baseline ripple. We have carried out an extensive analysis of the 774 GHz data, for which the O_2 line is accompanied by a moderately large range of frequencies without expected significant lines. We have data taken in 2010 March and September with a total of 26,848 s integration time. The noise (or fluctuation) bandwidth of the channels of the wideband spectrometer (WBS) used to obtain these data is determined by the channel frequency response, which is a quasi-Lorentzian function (Tolls et al. 2004). The resulting noise bandwidth is $\delta\nu_{\rm noise} = 1.62$ MHz and the nominal channel spacing is 0.57 MHz. This will vary slightly from the intrinsic spectrometer value due to shifting of channels in the frequency calibration procedure.

To clarify the comparison between theory and measurements, we have boxcar smoothed the data to a bandwidth of 2 MHz. According to the simple formula for the noise bandwidth for combination of channels (Ossenkopf 2008; Schieder & Kramer 2001) the noise bandwidth in this case should be close to 3 MHz. We utilize the single-sideband extracted spectra as described above, giving us a theoretical rms noise for a switched observation $\sigma(T_{\rm MB}) = 4T_{\rm noise}({\rm DSB})\epsilon_{\rm MB}^{-1}/\sqrt{\delta\nu_{\rm noise}t_{\rm int}}$, where $T({\rm DSB})$ is the double-sideband noise temperature, $\delta\nu_{\rm noise}$ is the noise bandwidth, and $t_{\rm int}$ is the total (on + off) integration time. We use for all the data $\epsilon_{\rm MB} = 0.75$, $T({\rm DSB}) = 179$ K for the V polarization channel, and $T({\rm DSB}) = 192$ K for the H polarization channel. The noise temperatures varied by only a few K over the six-month interval spanned by the observations.

We obtain for the V data $\sigma = 0.0062$ K, and for the H data $\sigma = 0.0053$ K, compared to theoretical values 0.0034 K and 0.0036 K, respectively. The ratio of observed to theoretical noise is 1.82 for V and 1.47 for H, with an average value of 1.65. These results are impacted by the difficulty of accurately

determining the rms from data due to the limited number of "clean" channels and time-dependent baselines, but they do indicate that the system performance is reasonably close to theoretical.

The correctness of the noise bandwidth is confirmed by comparison of data smoothed to 4 MHz channel width (5 MHz noise bandwidth) with the 2 MHz channel bandwidth (3 MHz noise bandwidth) data; the ratios for the different data sets have a mean value of 0.76 compared to 0.78 ($\sqrt{3/5}$) expected. The rms of the 4 MHz smoothed data is 0.0050 K for the V channel and 0.0036 K for the H channel, which average to a factor 1.61 times greater than the theoretical value. These results suggest that combining spectral channels reduces the noise in a manner close to that theoretically expected and that the overall level of fluctuations is a factor ~1.6 greater than that expected strictly from the radiometer equation for integration times up to 2.7×10^4 s.

APPENDIX B

EFFECT OF BEAM DILUTION ON LINE INTENSITY RATIOS

In general, the integrated antenna temperature, I, can be written

$$I = \int T_A dv = A_e \frac{A_{ul} N_u hc}{8\pi k} \int P_n(\Omega) C_n(\Omega) d\Omega, \quad \text{(B1)}$$

where, in addition to symbols defined following Equation (1), we have the antenna effective area A_e, the normalized antenna response pattern P_n, and the normalized column density distribution, C_n. For an extended uniform ($C_n = 1$) source filling the entire antenna pattern, the integral is the antenna solid angle, Ω_A. If the source is uniform but extended only to fill the main beam, the integral is the main beam solid angle, $\Omega_{\rm MB}$. The main beam efficiency $\epsilon_{\rm MB}$ is defined as $\epsilon_{\rm MB} = \Omega_{\rm MB}/\Omega_A$.

We can still use Equation (B1) by considering it to refer to a source that covers at most only the main beam, and a main beam-corrected integrated antenna temperature, $I_{\rm MB} = \epsilon_{\rm MB}^{-1} \int T_A dv$. From the antenna theorem, $A_e \Omega_A = \lambda^2$, for a given antenna. Then we can rewrite Equation (B1) as

$$I_{\rm MB} = \frac{A_{ul} N_u hc\lambda^2}{8\pi k} \frac{1}{\Omega_{\rm MB}} \int_{\rm MB} P_n(\Omega) C_n(\Omega) d\Omega, \quad \text{(B2)}$$

where the integral extends over the main beam. For a uniform source filling the main beam, the integral is just $\Omega_{\rm MB}$ and the integrated main beam temperature, $I_{\rm MB}^F$ is equal to the upper level column density multiplied by some constants,

$$I^{\rm src} = \frac{A_{ul} N_u hc\lambda^2}{8\pi k}, \quad \text{(B3)}$$

where we use the superscript src to indicate that this intensity is essentially a characteristic of the source itself rather than of the antenna being used for the observations. For a uniform small source located in the direction of the antenna boresight, $C_n = 1$ within the extent of the source and $= 0$ outside. The integral, which is nonzero over a range that is much smaller than the main beam size so $P_n = 1$, is equal to the source solid angle, Ω_S. Thus, the observed intensity denoted by the superscript obs is given by

$$I^{\rm obs} = \frac{A_{ul} N_u hc\lambda^2}{8\pi k} \frac{\Omega_S}{\Omega_{\rm MB}}. \quad \text{(B4)}$$

The ratio of the observed intensity to that of the source is given by

$$R = I^{\rm obs}/I^{\rm src} = \Omega_S/\Omega_{\rm MB}. \quad \text{(B5)}$$

Using the antenna theorem again, and defining the aperture efficiency in terms of the physical area of the antenna through $A_e = \epsilon_A A_p$ we find

$$R = \frac{\epsilon_A}{\epsilon_{\rm MB}} A_p \Omega_S \lambda^{-2}. \quad \text{(B6)}$$

A low-frequency (larger wavelength) transition has a small value of R, which can be thought of as arising from the small filling factor at the low frequency where the beam size is larger. To analyze our *Herschel* observations of O_2 in a reasonably simple manner, we consider a "small" source to be one that is smaller than the beam sizes at all three observing frequencies. Assuming a constant ratio of aperture to main beam efficiency, which is quite good for *Herschel* (Olberg 2010), R for two different transitions, 2 and 1, can be written as

$$R(2/1) = [\lambda(1)/\lambda(2)]^2. \quad \text{(B7)}$$

REFERENCES

Acharyya, K., Fuchs, G. W., Fraser, H. J., van Dishoeck, E. F., & Linnartz, H. 2007, A&A, 466, 1005
Bally, J., Cunningham, N. J., Moeckel, N., et al. 2011, ApJ, 727, 113
Beckwith, S., Persson, S. E., Neugebauer, G., & Becklin, E. E. 1978, ApJ, 223, 464
Bergin, E. A., Langer, W. D., & Goldsmith, P. F. 1995, ApJ, 441, 222
Bergin, E. A., Melnick, G. J., & Neufeld, D. A. 1998, ApJ, 499, 777
Bergin, E. A., Melnick, G. J., Stauffer, J. R., et al. 2000, ApJ, 539, L129
Bergman, P. 1995, ApJ, 445, L167
Black, J. H., & Smith, P. L. 1984, ApJ, 277, 562
Boogert, A. C. A., Blake, G. A., & Tielens, A. G. G. M. 2002, ApJ, 577, 271
Burton, M. G., & Haas, M. R. 1997, A&A, 327, 309
Carty, D., Goddard, A., Köhler, S. P. K., Sims, I. R., & Smith, I. W. M. 2006, J. Chem. Phys. A, 110, 3101
Chièze, J. P., & Pineau des Forêts, G. 1989, A&A, 221, 89
Chrysostomou, A., Burton, M. G., Axon, D. J., et al. 1997, MNRAS, 289, 605
Collings, M. P., Anderson, M. A., Chen, R., et al. 2004, MNRAS, 354, 1113
Combes, F., Casoli, F., Encrenaz, P., & Gerin, M. 1991, A&A, 248, 607
Combes, F., & Wiklind, T. 1995, A&A, 303, L61
Combes, F., Wiklind, T., & Nakai, N. 1997, A&A, 327, L17
Corey, G. C., Alexander, M. H., & Schaefer, J. 1986, J. Chem. Phys., 85, 2726
de Graauw, Th., Helmich, F. P., Phillips, T. G., et al. 2010, A&A, 518, L6
Downes, D., Genzel, R., Becklin, E. E., & Wynn-Williams, C. G. 1981, ApJ, 244, 869
Erickson, N. R., Goldsmith, P. F., Snell, R. L., et al. 1982, ApJ, 261, L103
Favre, C., Despois, D., Brouillet, N., et al. 2011, arXiv:1103.2548v1
Fraser, H. J., Collings, M. P., McCoustra, M. R. S., & Williams, D. A. 2001, MNRAS, 327, 1165
Frayer, D. T., Seaquist, E. R., Thuan, T. X., & Sievers, A. 1998, ApJ, 503, 231
Fuente, A., Cernicharo, J., García-Burillo, S., & Tejero, J. 1993, A&A, 275, 558
Gezari, D. Y., Backman, D. E., & Werner, M. W. 1998, ApJ, 509, 283
Goicoechea, J. R., Cernicharo, J., Lerate, M., et al. 2006, ApJ, 641, L49
Goldsmith, P. F., & Langer, W. D. 1978, ApJ, 222, 881
Goldsmith, P. F., Li, D., Bergin, E. A., et al. 2002, ApJ, 576, 831
Goldsmith, P. F., Melnick, G. J., Bergin, E. A., et al. 2000, ApJ, 539, L123
Goldsmith, P. F., Snell, R. L., Erickson, N. R., et al. 1985, ApJ, 289, 613
Goldsmith, P. F., & Young, J. S. 1989, ApJ, 341, 718
Graedel, T. E., Langer, W. D., & Frerking, M. A. 1982, ApJS, 48, 321
Gustafsson, M., Kristensen, L. E., Clénet, Y., et al. 2003, A&A, 411, 437
Harding, L. B., Maergoiz, A. I., Troe, J., & Ushakov, V. G. 2000, J. Chem. Phys., 113, 11019
Herbst, E., & Klemperer, W. 1973, ApJ, 185, 505
Hirota, T., Bushimata, T., Choi, Y. K., et al. 2007, PASJ, 59, 879
Hollenbach, D., Kaufman, M. J., Bergin, E. A., & Melnick, G. J. 2009, ApJ, 690, 1497
Howard, M. J., & Smith, I. W. M. 1981, J. Chem. Soc. Faraday Trans. 2, 77, 997

Ioppolo, S., Cuppen, H. M., Romanzin, C., van Dishoeck, E. F., & Linnartz, H. 2008, ApJ, 686, 1474
Ioppolo, S., Cuppen, H. M., Romanzin, C., van Dishoeck, E. F., & Linnartz, H. 2010, Phys. Chem. Chem. Phys., 12, 12065
Jensen, M. J., Bilodeau, R. C., Safvan, C. P., et al. 2000, ApJ, 543, 764
Kaufman, M. J. 2010, Talk at The Stormy Cosmos: The Evolving ISM from Spitzer to Herschel and Beyond, 2010 November, available at, http://www.ipac.caltech.edu/ism2010/sched.shtml
Kim, M. K., Hirota, T., Honma, M., et al. 2008, PASJ, 60, 991
Kristensen, L. E., Gustafsson, M., Field, D., et al. 2003, A&A, 412, 727
Lacombe, F., Gendron, E., Rouan, D., et al. 2004, A&A, 417, L5
Langer, W. D., & Graedel, T. E. 1989, ApJS, 69, 241
Larsson, B., Liseau, R., Pagani, L., et al. 2007, A&A, 466, 999
Le Bourlot, J., Pineau des Forêts, G., & Roueff, E. 1995, A&A, 297, 251
Leung, C. M., Herbst, E., & Heubner, W. F. 1984, ApJS, 56, 231
Lique, F. 2010, J. Chem. Phys., 132, 044311
Lique, F., Jorfi, M., Honvault, P., et al. 2009a, J. Chem. Phys., 131, 221104
Lique, F., van der Tak, F. F. S., Kłos, J., Bulthuis, J., & Alexander, M. 2009b, A&A, 493, 557
Liseau, R., Larsson, B., Bergman, P., et al. 2010, A&A, 510, A98
Liszt, H. S. 1985, ApJ, 298, 281
Liszt, H. S. 1992, ApJ, 386, L139
Liszt, H. S., & Vanden Bout, P. A. 1985, ApJ, 291, 178
Luhman, M. L., Jaffe, D. T., Keller, L. D., & Pak, S. 1994, ApJ, 436, 185L
Maréchal, P., Pagani, L., Langer, W. D., & Castets, A. 1997a, A&A, 318, 252
Maréchal, P., Viala, Y. P., & Benayoun, J. J. 1997b, A&A, 324, 221
Maréchal, P., Viala, Y. P., & Pagani, L. 1997c, A&A, 328, 617
Masson, C. R., & Mundy, L. G. 1988, ApJ, 324, 543
Melnick, G. J., Stauffer, J. R., Ashby, M. L. N., et al. 2000, ApJ, 539, L77
Menten, K. M., Reid, M. J., Forbrich, J., & Brunthaler, A. 2007, A&A, 474, 515
Miyauchi, N., Hidaka, H., Chigai, T., et al. 2008, Chem. Phys. Lett., 456, 27
Mul, P. M., McGowan, J. W., Defrance, P., & Mitchell, J. B. A. 1983, J. Phys. B, 16, 2099
Müller, H. S. P., Thorwith, S., Roth, D. A., & Winnewisser, G. 2001, A&A, 370, L49
Murata, Y., Kawabe, R., Ishiguro, M., Hasegawa, T., & Hayashi, M. 1991, in IAU Symp. 147, Fragmentation of Molecular Clouds and Star formation, ed. E. Falgarone, F. Boulanger, & G. Duvert (Dordrecht: Kluwer), 357
Murata, Y., Kawbe, R., Ishiguro, M., et al. 1992, PASJ, 44, 381
Neau, A., Al Khalili, A., Rosén, S., et al. 2000, J. Chem. Phys., 11, 1762
Nenkova, M., Ivezić, Ž, & Elitzur, M. 2000, in ASP Conf. Ser. 196, Proc. Conf. Thermal Emission Spectroscopy and Analysis of Dust, Disks, and Regoliths, ed. M. Sitko, A. Sprague, & D. Lynch (San Francisco, CA: ASP), 77
Nordh, H. L., von Schéele, F., Frisk, U., et al. 2003, A&A, 402, L21
Öberg, K. I., Linnartz, H., Visser, R., & van Dishoeck, E. F. 2009a, ApJ, 603, 1209
Öberg, K. I., van Dishoeck, E. F., & Linnartz, H. 2009b, A&A, 496, 281
Olberg, M. 2010, HIFI ICC Technical Note ICC/2010-nnn, issue 1.1
Olofsson, G., Pagani, L., Tauber, J., et al. 1998, A&A, 339, L81
Orlikowski, T. 1985, Mol. Phys., 56, 35
Ossenkopf, V. 2008, A&A, 479, 215
Ott, S. 2010, in ASP Conf. Ser. 434, Astronomical Data Analysis Software and Systems XIX, ed. Y. Mizuno, K. I. Morita, & M. Ohishi (San Francisco, CA: ASP), 139
Pagani, L., Langer, W. D., & Castets, A. 1993, A&A, 274, L13
Pagani, L., Olofsson, A. O. H., Bergman, P., et al. 2003, A&A, 402, L77
Pardo, J. R., Cernicharo, J., & Phillips, T. G. 2005, ApJ, 634, L31
Parmar, P. S., Lacy, J. H., & Achtermann, J. M. 1994, ApJ, 430, 786
Pauls, T. A., Wilson, T. L., Bieging, J. H., & Martin, R. N. 1983, A&A, 124, 23
Penzias, A. A. 1981, ApJ, 249, 518
Pilbratt, G. L., Riedinger, J. R., Passvogel, T., et al. 2010, A&A, 518, L1
Plambeck, R. L., & Wright, M. C. H. 1987, ApJ, 317, L101
Pontoppidan, K. M., Fraser, H. J., Dartois, E., et al. 2003, A&A, 408, 981
Prasad, S. S., & Huntress, W. T., Jr. 1980, ApJS, 43, 1
Quémener, G., Balakrishnan, N., & Kendrick, B. K. 2008, J. Chem. Phys., 129, 224309
Rosenthal, D., Bertoldi, F., & Drapatz, S. 2000, A&A, 356, 705
Salas, L., Rosado, M., Cruz-González, I., et al. 1999, ApJ, 511, 822
Sandqvist, Aa., Larsson, B., Hjalmarson, Å., et al. 2008, A&A, 482, 849
Sandstrom, K. M., Peek, J. E. G., Bower, G. C., Bolatto, A. D., & Plambeck, R. L. 2007, ApJ, 667, 1161
Schieder, R., & Kramer, C. 2001, A&A, 373, 746
Schild, H., Miller, S., & Tennyson, J. 1997, A&A, 318, 608
Schöier, F. L., van der Tak, F. F. S., van Dishoeck, E. F., & Black, J. H. 2005, A&A, 432, 369
Scoville, N. Z., Hall, D. N. B., Kleinmann, S. G., & Ridgway, S. T. 1982, ApJ, 253, 136
Shultz, A. S. B., Colgan, S. W. J., Erickson, E. F., et al. 1999, ApJ, 511, 282
Smith, I. W. M., & Stewart, D. W. A. 1994, J. Chem. Soc. Faraday Trans. 2, 90, 3221
Smith, P. L., Griesinger, H. E., Black, J. H., Yoshino, K., & Freeman, D. E. 1984, ApJ, 277, 569
Stolovy, S., Burton, M. G., Erickson, E. F., et al. 1998, ApJ, 492, L151
Tolls, V., Melnick, G. J., Ashby, M. L. N., et al. 2004, ApJS, 152, 137
Valkenberg, R. 1995, Diplom. in Physik thesis, Rheinisch–Westfälischen Tech. Hochschule, Aachen
Vandenbussche, B., Ehrenfreund, P., Boogert, A. C. A., et al. 1999, A&A, 346, L57
Van der Tak, F. F. S., Black, J. H., Schöier, F. L., Jansen, D. J., & van Dishoeck, E. F. 2007, A&A, 468, 627
Vannier, L., Lemaire, J. L., Field, D., et al. 2001, A&A, 366, 651
Vejby-Christensen, L., Andersen, L. H., Heber, O., et al. 1997, ApJ, 483, 531
Wakelam, V., Selsis, F., Herbst, E., & Caselli, P. 2005, A&A, 444, 883
Whittet, D. C. B. 2010, ApJ, 710, 1009
Wilson, C. D., Olofsson, A. O. H., Pagani, L., et al. 2005, A&A, 443, L5
Wilson, T. L., Gaume, R. A., Gensheimer, P., & Johnston, K. J. 2000, ApJ, 538, 665
Wright, M. C. H., Plambeck, R. L., & Wilner, D. J. 1996, ApJ, 469, 216
Wright, M. C. H., Sandell, G., Wilner, D. J., & Plambeck, R. L. 1992, ApJ, 393, 225
Xie, T., Allen, M., & Langer, W. D. 1995, ApJ, 440, 674
Xu, C., Xie, D., Honvault, P., Lin, S. Y., & Guo, H. 2007, J. Chem. Phys., 127, 024304